U.S.N.A.---Trident Scholar project report; no. XXX (2003)

PHYSICAL PROPERTIES OF NEAR-EARTH OBJECTS: OPTICAL AND INFRARED ASTRONOMICAL OBSERVATIONS

by

Midshipman Luke R. Dundon, Class of 2003
United States Naval Academy
Annapolis, Maryland

_____
(signature)

Certification of Adviser Approval

Associate Professor Debora M. Katz
Physics Department

_____
(signature)

_____
(date)

Acceptance for the Trident Scholar Committee

Professor Joyce Shade
Deputy Director of Research & Scholarship

_____
(signature)

_____
(date)

USNA-1531-2

REPORT DOCUMENTATION PAGE

Form Approved
OMB No. 074-0188

1. AGENCY USE ONLY (Leave blank)	2. REPORT DATE	3. REPORT TYPE AND DATE COVERED
	30 April 2003	

4. TITLE AND SUBTITLE
Physical properties of near-Earth objects : optical and infrared astronomical observations

5. FUNDING NUMBERS

6. AUTHOR(S)
Dundon, Luke R. (Luke Rupert), 1981-

7. PERFORMING ORGANIZATION NAME(S) AND ADDRESS(ES)		8. PERFORMING ORGANIZATION REPORT NUMBER

9. SPONSORING/MONITORING AGENCY NAME(S) AND ADDRESS(ES)		10. SPONSORING/MONITORING AGENCY REPORT NUMBER
US Naval Academy Annapolis, MD 21402		**Trident Scholar project report no. 306 (2003)**

11. SUPPLEMENTARY NOTES

12a. DISTRIBUTION/AVAILABILITY STATEMENT	12b. DISTRIBUTION CODE
This document has been approved for public release; its distribution is UNLIMITED.	

13. ABSTRACT: Trident Scholar Project constrained the intrinsic physical properties of a sample of recently discovered NEOs. The sample was carefully chosen based on the NEOs' proper motion1, magnitude and position. Two weeks in Arizona were spent making thorough optical and infrared ground-based observations on the sample. Four telescopes were used: 1) the Kitt Peak National Observatory's 2.1-meter telescope with the Simultaneous Quad Infrared Imaging Device, 2) the University of Arizona's 2.3-meter Steward optical observatory, 3) Spacewatch's 1.8-meter optical telescope and 4) the 0.5-meter Super Livermore Optical Transient Imaging System automatic telescope. These instruments were used to measure color photometry in six different bandpasses, and to make optical and infrared lightcurves. The optical and infrared lightcurves were analyzed to determine the rotational properties and rough shape of each object. The taxonomic classification was constrained from three-color optical photometry, three-color infrared photometry, broadband spectra and albedo. From these taxonomic classifications, a chemical composition was assigned to each object. Four out of the five objects were classified as silicon-iron based NEOs, and one was classified as a potential rare carbonaceous NEO. The determined periods ranged from 2-12 hours, and the shapes ranged from spherical to ellipsoidal.

14. SUBJECT TERMS:	15. NUMBER OF PAGES
asteroids, near-earth asteroids, optical observations, infrared observations	**80**
	16. PRICE CODE

17. SECURITY CLASSIFICATION OF REPORT	18. SECURITY CLASSIFICATION OF THIS PAGE	19. SECURITY CLASSIFICATION OF ABSTRACT	20. LIMITATION OF ABSTRACT

ABSTRACT

The majority of asteroids and comets are far from Earth. A few known as Near-Earth Objects (NEOs) are on orbits that bring them close to this planet. Their close proximity permits more detailed observations, yet also makes them a threat to the biosphere. Despite their relevance, the physical properties of these objects have not been widely studied.

The Trident Scholar Project constrained the intrinsic physical properties of a sample of recently discovered NEOs. The sample was carefully chosen based on the NEOs' proper motion[1], magnitude and position. Two weeks in Arizona were spent making thorough optical and infrared ground-based observations on the sample. Four telescopes were used: 1) the Kitt Peak National Observatory's 2.1-meter telescope with the Simultaneous Quad Infrared Imaging Device, 2) the University of Arizona's 2.3-meter Steward optical observatory, 3) Spacewatch's 1.8-meter optical telescope and 4) the 0.5-meter Super Livermore Optical Transient Imaging System automatic telescope. These instruments were used to measure color photometry in six different bandpasses, and to make optical and infrared lightcurves.

The optical and infrared lightcurves were analyzed to determine the rotational properties and rough shape of each object. The taxonomic classification was constrained from three-color optical photometry, three-color infrared photometry, broadband spectra and albedo. From these taxonomic classifications, a chemical composition was assigned to each object. Four out of the five objects were classified as silicon-iron based NEOs, and one was classified as a potential rare carbonaceous NEO. The determined periods ranged from 2-12 hours, and the shapes ranged from spherical to ellipsoidal.

Key Words: asteroids, near-earth asteroids, optical observations, infrared observations

[1] Proper motion refers to the velocity tangential to the plane of the sky. This motion can be observed with ground-based telescopes.

ACKNOWLEDGEMENTS

I would like to extend my sincere gratitude and appreciation to Associate Professor Debora Katz for all her tremendous wisdom and mentorship. I would also like to thank Dr. Jeffrey Larsen at Spacewatch for his incredible assistance in offering guidance and advice throughout the course of the observing run at Kitt Peak and during the analysis at USNA. Equally vital to the success of this project were the guidance and aid given by the staff at Kitt Peak National Observatory, Arizona. This work would also not have been possible without the help of people such as Ms. Lisa Becktold of the CADIG computer department. I would additionally like to thank the Trident Scholar Committee, Professor Joyce Shade, Dean William Miller, and the United States Naval Academy Physics Department for allowing me to do this project.

TABLE OF CONTENTS

1. INTRODUCTION

Tumbling overhead are fossil records of the early Solar System. Near-Earth Objects (NEOs) have influenced the history of this planet. Life itself has been molded and re-shaped by the very behavior of these objects, and it could be shaped again in the future. NEOs are asteroids and comets whose orbits either cross Mars' orbit or lie completely inside Mars' orbit (Cunningham 1988).

While the proximity of NEOs makes them relatively easy to observe, it also makes them a potential hazard. For example, on August 18, 2002, a newly discovered Near-Earth Object, 2002 NY40,[2] was only 1.3 lunar distances from Earth. On a cosmological scale, that distance is minuscule. Last year eight NEOs came within three lunar distances. A collision with one of these objects could destroy the biosphere. Because these objects pose such a great threat to the Earth, further studies are critical to the survival of humanity (Lupishko 2000).

In addition to the threat they pose, NEOs may be very useful. In future years, with advances in space exploration technology, these objects could be mined for their abundant mineral resources. This mining may be vital for the advancement of space exploration by supplying raw materials that do not need to be launched from Earth (Lupishko 2000).

While NEOs are interesting, threatening and potentially useful, little attention has been given to these bodies. These objects are the least studied in astronomy and astrophysics research (Binzel 1989). Because of the need for further investigation of these objects, the goal of this project was to study the physical properties of a sample of NEOs.

---

[2] Near-Earth Asteroids are labeled based upon the time that they are discovered. 2002 NY40, for example, was discovered in the year 2002. "N" indicates it was discovered in the seventh month of the year, and "Y" indicates that it was discovered in the second half of the month. "40" indicates it was the 40th asteroid discovered during this 2-week interval.

1.1 NEOs AND THEIR HISTORICAL IMPORTANCE

Studying the physical properties of NEOs will help reveal the evolutionary history of the Solar System. Near-Earth Asteroids are fossils that contain evidence of the formation of the planets and the distribution of the elements. Their composition contains the building blocks of life on Earth, such as amino acid complexes and hydrocarbons (Binzel 1989). The asteroids are among those objects in the Solar System that have not changed due to plate tectonics since their original formation. Gathering information on the early history of the Solar System through the study of meteorites (chunks of asteroids which strike Earth's surface), requires understanding the formation and evolution of the asteroid bodies themselves (Wetherill and Chambers 1999).

The key to unlocking the fossil records contained within NEOs is determining their physical properties. During the Solar System's formation, planetesimals accreted and formed the planets. The NEOs of today are essentially planetesimals that did not come together to form planets. As these objects are closer to Earth than the Main Belt Asteroids, NEOs provide an important opportunity for investigation. Knowing the physical properties of these objects will help to determine the composition of the interiors of planets and satellites (Bell et al. 1985). The physical properties of asteroids and comets are valuable because the interiors of a planet cannot be seen, but NEOs and especially those whose interiors have been exposed by collisions can be observed.

1.2 EVOLUTION OF LIFE ON EARTH

The evolution of Earth has been strongly affected by the impacts of many comets and asteroids with the planet's surface (Alvarez et al. 1980). Cometary impacts are believed to be

responsible for providing the Earth with water and key elements in the atmosphere, while asteroids probably delivered several different molecular compounds, such as those needed for sustaining life (e.g., Chyba 1990, Hunten 1993).

Ironically, these objects that may have provided much of the materials needed for life on Earth may also upon occasion have caused the extinction of whole species of animals. One example was the object that struck the Yucatan peninsula in Mexico 65 million years ago. It is likely that this event caused the extinction of over 75% of the Earth's living organisms, including the dinosaurs (e.g., Grieve & Shoemaker 1994). Many mammals then were small creatures that survived the catastrophic impact. With many of their larger competitors destroyed, the mammals dominated the Earth. Consequently, the evolution of humanity may be due in part to Earth's history of collisions with NEOs.

1.3 NEO THREAT: CURRENT AND FUTURE

Although the overall probability of impact with the Earth at any one instant is very low, the threat of impact from these objects hurtling through space is just as real now as it was during the age of the dinosaurs. Every day, about one hundred tons of interplanetary material drifts through the Earth's atmosphere. Every 100 years an asteroid about 50 meters in diameter is expected to hit the surface of the Earth, causing local disasters on the planet, as could have been the case with 2002 NY40. Such a case did occur in the Tunguska incident of 1908, where an NEO impacted a rural region of Siberia. Widespread damage resulted for miles. Every few hundred thousand years, asteroids larger than a kilometer could cause a global disaster. Such a collision could result in the extinction of the human race (Morrison et al. 1992).

1.4 NEO MINING FOR RESOURCES

In addition to being potential threats to humanity, NEOs could one day be utilized for their abundance of resources. Knowing the chemical composition will be important in exploiting NEOs for their natural resources (Cunningham 1988). Most NEOs are asteroids; only 5% are extinct comets. As explained in sections 6-8, several properties are observed in order to place Near-Earth Asteroids in a taxonomic bin, which is correlated with chemical composition.[3] Previous research indicates that most Near-Earth Asteroids are 75% C-type (carbonaceous), 20% S-type (iron-silicate), 1-2% M-type (metallic) or 1-2% D-type (low-brightness, primitive; Binzel 1989).

Presently, it is not cost-effective to mine these minerals and bring them back to Earth. However, these materials could be used to develop space structures and generate rocket fuel that will be required to explore and colonize the Solar System (Shoemaker et al. 1995). Asteroids are composed of a wide variety of materials including iron-nickel alloy, precious metals, organic chemicals, and chemically bound oxygen. Obviously, determining the taxonomic class of the asteroid by studying the physical properties of the object will aid in exploiting the object's natural resources. NEO exploitation would require less energy than a Moon landing, making them the cheapest targets beyond the Moon for robotic or possibly human exploration (Shoemaker et al. 1995).

---

[3] This classification system actually includes D, R, V, A, S, B, C, F, G, D, T and Q asteroids. C-type is carbonaceous, and includes over 75% of known asteroids. The C-types are very dark with low albedo (brightness), and the composition is thought to be depleted in hydrogen, helium and other volatiles. These asteroids mainly inhabit the Main Belt's outer regions. The S-type has high concentrations of silicate, and accounts for approx. 20% of known asteroids. They have moderate brightness, and their composition is mixed with iron and iron-silicate minerals. These asteroids dominate the inner asteroid belt, closer to the Earth (consequently the largest percentage of NEOs). M-type is metallic, and basically includes the rest of the known asteroids (such as R, V, A, T, etc.). The brightness is the highest among these, and their composition is mainly metallic iron. They are concentrated in the Main Belt's middle region (Binzel 1989).

2. EXPERIMENTAL PROCEDURE

2.1 NEO SAMPLE

The selected sample of Near Earth Objects included asteroids that were recently discovered and had no determined properties. The only known properties of the sample were the absolute magnitude[4,5] (H), the proper motion and a rough diameter based on its H-magnitude. The speed of the imager on the telescope limited the proper motion of the object. If the NEO moved too quickly it would appear as a streak in the image. The NEO had to be above the horizon during the scheduled observing time and had to be bright enough to be imaged by the instruments.

The sample also contained two different orbital types, Apollo and Amor. Orbital types are classified by their distances of approaching Earth's orbit. Apollo orbits are those that cross the Earth's orbit. Amor orbits are located nearer Mars, and never come within the Earth's orbit. The discoverers of this sample (see Table 1) included Jet Propulsion Laboratory's Near-Earth Asteroid Tracking Program of Pasadena California, MIT's Lincoln Laboratory Near-Earth Asteroid Research program, and the Spacewatch project of the University of Arizona.

Once multiple images are taken of a source, one has to first find the moving object amongst consecutive images. This process is known as "blinking." Similar to a movie projector, a series of images are blinked on top of one another, and one looks to discover an object that is

---

[4] Magnitude (unitless in dimensions), is used to relate the brightness of an object on a logarithmic scale. The magnitude system originated with ancient Greek astronomers. In their system the brightest objects were assigned a magnitude of 1, the faintest magnitude 6. The system used today has been broadened to include objects beyond the limit of human vision and to allow for fractional magnitudes. In general f_a and f_b are fluxes in W/m^2, and the relation between corresponding magnitudes m_a and m_b is

$$m_b - m_a = 2.5\log(f_1/f_2)$$ (e.g., Binzel 1989).

[5] Assumed magnitude (brightness) of an object at 1 AU from both the Earth and the Sun. This magnitude is used for objects which have constantly changing orbits.

moving with respect to the star field, which is stationary. Usually the apparent brightness of the object is much less than the surrounding stars.

NEO	H-mag	Diameter (km)	Orbital Type	Discoverer & Date
2002 HK12	18.2	0.7-1.5	Apollo	JPL/NEAT April 30, 2002
2002 KH3	17.6	0.9-2.0	Amor	LINEAR May 17, 2002
2002 KH4	15.5	2.4-5.4	Amor	LINEAR May 22, 2002
2000 BF19	19.5	0.4-0.8	Apollo	Spacewatch Jan. 28, 2000
2002 PY39	21.4	0.15-0.35	Amor	JPL/NEAT Aug. 8, 2002

Table 1. NEO sample

2.2 OBSERVING PROCEDURES

A typical night of observing work was conducted from dusk until dawn. Detailed preparation for the next night's observation occurred during the afternoon hours, which included checking previous night's data, finding the ephemeris[6] for the sample as well as appropriate standard stars needed for calibration.

The observing run was concluded on four telescopes over a two-week period. Table 2 summarizes the general characteristics and time spent on each telescope.

[6] "Ephemeris" is the predicted location of an object in the sky based on its orbital elements and motion. The Minor Planet Center provides this computational service online. It contains a database on all known Near-Earth Asteroid discoveries made by astronomers.

Telescope	Diameter (meters)	Focal Ratio[7] & Description	Resolution[8]	Magnitude Limit[9]	Observing Time
2.1 Meter (KPNO)	2.1	f/2.63 Cassegrain	0.69"/pixel	19	1.5 nights Sept 16-18
Steward	2.3	f/2.66 Cassegrain	1.00"/pixel	22	3 nights Sept 19-21
Spacewatch	1.8	f/2.7 Prime Focus	1.00"/pixel	21	3 nights Sept 25-27
Super LOTIS	0.45	f/3.5 automatic drive	1.5"/pixel	19	3 nights Sept 19-21

Table 2. Telescope summary

When taking lightcurve data, it was important to remain focused on the source for substantial length of time. Otherwise, one could miss key parts of the object's rotation. Because there existed more than one member in the sample, each telescope was moved periodically from one object to the next. In order to gather sufficient data on each object, a relatively small sample was initially chosen. This net time was divided into intervals throughout the course of each night.

It was important to track these objects over intervals of time in order to measure their changes in magnitude. The variation in the brightness over time creates a curve, due to the changes in brightness caused by the different angles of the asteroid that face the Earth throughout its rotation (see Figures 14-36; Harris et al. 1989). The light given off by the asteroid is due to the reflection of sunlight off the face of the asteroid that is facing the Earth at a given point in time.

[7] The focal ratio is the ratio of the focus (distance of the mirror to the point in space where the light rays converge to form an image) to the aperture size of the mirror.
[8] The resolution is the number of arcseconds that each pixel represents on the raw image.
[9] "Magnitude Limit" is the faintest (thus largest) magnitude of light that the telescope can detect.

2.3 OBSERVATIONS

KPNO

In May of 2002, national telescope time was awarded on Kitt Peak National Observatory (KPNO). The awarded time on the KPNO telescope was scheduled from September 16 through September 18 (2.5 nights awarded by the National Optical Astronomical Observatory). While two observers worked at KPNO, Dr. Jeffrey Larsen made simultaneous optical observations on Spacewatch.

The KPNO telescope, with the Simultaneous Quad Infrared Imaging Device (SQIID), was used to make observations in the near-infrared. The SQIID imager has 440x460 pixels, translating to a 5.1 x 5.3 arcmin field-of-view. It is labeled "Simultaneous" and "Quad" because it can simultaneously take images at four infrared wavebands. These wavebands are J, H, K, and L. Unfortunately, the far-infrared L-band detector did not work as expected on the KPNO. This detector was completely saturated[10] in each image. Median wavelengths of the wavebands are given in Table 3.

Detector	Median Wavelength of Waveband (nm)
J	1200
H	1600
K	2200
L	3200

Table 3. Detectors used on SQIID imager

At most observatories, a technician or second operator was present for assistance. At the KPNO telescope, Associate Professor Debora Katz (Physics Department, USNA) acted as a telescope operator.

[10] "Saturated" refers to reaching the maximum limit of a pixel in the imager. Once this maximum count is reached, the pixel begins to spill charge into other nearby pixels. This causes some of the signal of the object to be lost in the imaging device.

Weather conditions on most nights were excellent, with the exception of high winds. These gusts were dangerous to the open domes of the telescopes. There was a storm on September 18, prohibiting data collection for that night on the KPNO and Spacewatch telescopes. Unfortunately, once time is allocated for a telescope, it is not re-allocated even in the event of bad weather. The first night was focused on training and learning the mechanisms of KPNO's elaborate SQIID camera. Consequently, only 2002 HK12 was tracked that night. The time-on-source for KPNO is given in Table 4.

Object	16-Sep	17-Sep	18-Sep
2002 HK12	2hr45min	0	30min
2002 KH3	0	0	2hr30min
2000 BF19	0	0	2hr40min

Table 4. Time on source for 2.1-meter telescope (KPNO)

In optical astronomy, a single image is taken each time the telescope is on-source, but in infrared astronomy several short exposures are taken. Between each short exposure the telescope is moved slightly. This technique is called "dithering." The dithering pattern established for the KPNO telescope involved five exposures. Between each exposure the telescope was shifted by 40 arcsec, creating a cross-like array of images, with the first of five being in the middle of the cross. The "empty" sky is bright in the infrared and its contribution must be subtracted from the images. In order to determine the sky's contribution, the other images are median-filtered. The "sky image" varies throughout the night.

The SQIID imager was equipped to co-add images. An exposure of 50 seconds could be broken into five 10-second exposures and then co-added by the processing computer. The same

signal could be accrued by keeping the shutter open for 50 seconds, but the noise and thermal emission would be much greater. By taking separate quick images and "co-adding" them, the noise is beneficially reduced.

Standard stars are required to calibrate the data. These standards must be observed using the same filters as the other sources and throughout the entire night. The standard stars used, P290-D, P247-U, and P247-Q, had published values in the J, H, and K wavebands. They were chosen based on their proximity to the sources of the sample.

STEWARD

During the observing run in September, additional time was granted on the other three telescopes. The 2.3-meter Steward Observatory, operated by the University of Arizona, was equipped with an optical CCD[11] camera and color filters. The size of the CCD is 1024x1024 pixels with a resolution of 1.00"/pixel, which gives a field-of-view of 16.4 x 16.4 arcmin. Even with such a size, the telescope had to be moved often to properly track the NEO's course through the night. The Steward filters are blue (B), green (V) and red (R; see Table 5).

Filter	Median Wavelength of Waveband (nm)
B	385
V	525
R	675

Table 5. Filters used by Steward Observatory

[11] CCD, or charge coupled device, is a digitally based camera that uses the photoelectric effect to register photons that strike the pixel well of the camera. From the impacts with this well, electron counts are registered. From these counts, the brightness and/or magnitude is calculated. CCDs are also found in common devices such as digital cameras.

Because each waveband saturated at different conditions and exposure times, filters also had different exposure times. The R-filter's long optical wavelength is the least scattered waveband in the Earth's atmosphere. It is also the most easily saturated; consequently, its exposure time was the shortest at 60-90 seconds for all images. Atmospheric extinction hampers the passage of blue light through the atmosphere. Therefore the B filter required that the shutter remain open approximately 150 seconds. Typical V-filter exposure times were 120 seconds.

Table 6 gives a summary of the time on source for Steward Observatory. Steward Observatory's CCD had a limiting magnitude of V=22. The object 2002 PY39 was chosen because it was visible and did not have documented information on its physical properties. It was not viewable through the KPNO telescope because of its faint infrared magnitude.

Steward observations of 2002 PY39 were used for both lightcurves and color measurements. An additional Near-Earth Object, 2002 KH4, was also included in the color measurements.

Object	19-Sep	20-Sep	21-Sep
2002 HK12	20 min	0	15min
2002 KH3	1hr 40min	1hr 40min	1hr 30min
2000 BF19	1hr 30min	1hr 15min	1hr 50min
2002 PY39	0	1hr 10min	1hr 35min
2002 KH4	0	20min	20min

Table 6. Time on source for 90-inch Steward telescope

SPACEWATCH

The 1.8-meter Spacewatch telescope was used to observe unfiltered lightcurves, especially of the fainter NEOs in the sample. The Spacewatch CCD is 2048 x 2048 pixels with a resolution of 1.00”/pixel. Its field of view is large (34 x 34 arcmin) so the telescope does not need to be moved as often to track the NEOs. This is important because the Spacewatch telescope was built from spare parts. The mirror on this telescope was originally built for a space telescope. It has nine drive motors that often work at cross-purposes and cause the telescope to drift and slip. The telescope has an azimuth-elevation mount, different from KPNO or Steward. This mount combined with the motors means that Spacewatch has difficulty staying on source near the zenith.

From September 16-18, Dr. Larsen at the Spacewatch telescope took simultaneous optical measurements on the sample while KPNO took infrared measurements. Spacewatch telescope’s optical data, combined with the KPNO infrared data, was used for albedo calculations (further explanation in section 6). This telescope offered an additional opportunity to gather optical lightcurve data. Table 7 gives times-on-source at Spacewatch for each of these objects after Dr. Larsen’s simultaneous observations.

Object	26-Sep	27-Sep
2002 HK12	30min	30min
2002 KH3	50min	40min
2000 BF19	40min	0

Table 7. Time on source for Spacewatch 1.8-meter telescope

SUPER-LOTIS

The Super-LOTIS (Livermore Optical Transient Imaging System) 16-inch automatic telescope simultaneously took optical unfiltered lightcurves for four nights on 2002 HK12. Its large field of view (34 x 34 arcmin) allowed it to remain stationary with respect to the starfield throughout the night. It has poor resolution at 1.5"/pixel and had a limiting magnitude brighter than that of the other telescopes. Like Spacewatch, it also had an unfiltered CCD. While attempts at tracking potential candidates 2002 KH4 and 2002 RQ25 failed on Super-LOTIS, 2002 HK12 was successfully observed on the nights of September 20 and 22. It was noted here the importance of the astronomer at the telescope *during* the observations. An astronomer would have stopped trying to observe objects that did not appear in the images.

3. DATA REDUCTION

Before photometry[12] was performed on the sample, the images were first *cleaned* or *reduced* from noise due to the sky and the camera itself. Cleaning a raw image involves dark image subtraction, sky image subtraction, and flat-field division. Dark images were obtained with the KPNO infrared and optical CCDs by taking exposures with the shutter closed. This dark image subtraction accounts for the noise from the electrical current of the instrument. For infrared measurements, sky images need to be subtracted due to noise from the sky. Sky subtraction is not needed for optical images, where the sky background is negligible.

Each pixel well in the CCD camera is structured slightly differently than its neighboring pixels. Even when the same number of photons are collected by each pixel, these pixels will each register slightly different magnitudes of light. A flat-field (image with uniform brightness

[12] "Photometry" is the measurement of the brightness of light.

across all pixels) is used to normalize these different responses. The infrared flat-field is constructed from a median combination of a group of sky images. For the optical CCD, a flat-field is made by observing an evenly illuminated screen. In addition, a bias is subtracted from the optical flat-field image. This bias accounts for the pre-charge on the pixels in the camera before the shutter is opened. The infrared flat-field automatically subtracts a bias when it subtracts a dark image from itself.

The following expresses this process mathematically for an infrared image:

$$C = \frac{R - S}{F - D} \qquad \text{(Eq. 1)}$$

where C is the cleaned image, R is the raw image, S is the sky image, F is the flat-field, and D is the dark image.

The following expression is for reduction of a raw optical image:

$$C = \frac{R - D}{F - B} \qquad \text{(Eq. 2)}$$

where B is the bias image.

Images of longer exposure times have larger thermal noise from the electrical current of the camera itself. For infrared images, the flat is composed of sky images, which are themselves made from raw images. Consequently, the flat-field must be subtracted by a dark image. In the optical, the flat is only an exposure of approximately one second; consequently, it does not need a dark subtraction.

The standard Unix-based computer program used to calculate photometry was IRAF (Image Reduction and Analysis Facility). IRAF has a photometry package that required many inputs, among which included the “radius of aperture,” “sky fitting radius,” and “zero-magnitude

point" (similar to the ground of a voltmeter). The radius of aperture indicated how many pixels would be measured, and the sky-fitting radius indicated how many outside pixels would be used for sky subtraction (minimal in the optical images). Researchers usually use a radius 4-5 times the size of the Full-Width Half-Maximum of the source object's radial profile (Davis 1989). The sky-fitting radius was chosen in all images to be five pixels beyond the inner aperture radius.

4. CALIBRATION OF DATA

Once reduced, the images need to be standardized before performing photometry. Photometry is a process of assigning a magnitude to the object. However, there must be a way of standardizing the magnitudes of each image. While tracking the asteroid, a nearby standard star that has a published magnitude was also tracked. The observed magnitude of the standard was not the same as its published value due to atmospheric extinction. Earth's atmosphere scatters light in the blue waveband, causing objects to appear redder and fainter than they truly are (e.g., Karttunnen et al. 1987). The measured difference between observed and published magnitude of the standard star gave the correction that was applied to the NEO. The star was tracked through the night because the atmospheric extinction of any object differs based on its location in the sky, as shown in Figure 1.

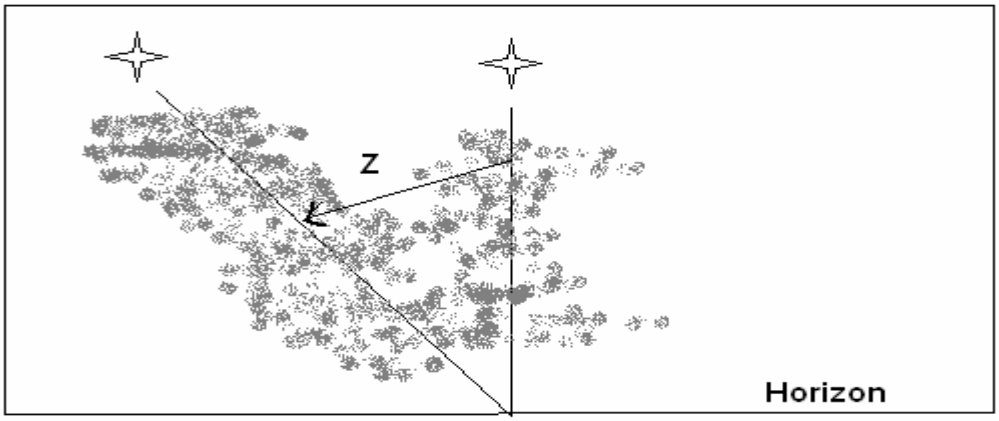

Figure 1. Different airmasses at different viewing angles

As can be seen in Figure 1, one would be looking through more airmass (represented by gray clouds) the closer the object is to the horizon. It is optimal to observe at no larger an airmass than two (where one correlates to zenith, and infinity correlates to the horizon; two corresponds to 60 degrees from zenith)[13]. By observing the star across the sky, an "extinction curve" is plotted, indicating the different corrections to be made for different airmasses (Hiltner 1964, Karttunen et al. 1987). This linear relationship of greater corrections for greater airmasses is then applied to the asteroid.

The extinction curves were constructed and applied for KPNO, Steward, and Spacewatch. These curves are shown in Figures 2-13. Each point has error bars; in many plots of this paper the error bars are smaller than the size of the data point. A different extinction curve is needed for each night and for each filter (Baschek et al. 1991). The equations listed at the top of each plot reflect the extinction correction equation to be applied to the asteroid for that night, in that filter. Super-LOTIS was used primarily for rotational period determinations, and consequently did not need any extinction curves for calibration.

[13] The airmass equation is X=sec(1/Z), where X=airmass and Z=the angle from zenith.

Error bars on all plots in this paper were estimated assuming a Poisson distribution of the error in each measurement. The error in magnitude was calculated from

$$\sigma = \frac{\sqrt{N}}{N}, \qquad \text{(Eq. 3)}$$

where σ equals the error and *N* equals the number of counts that constitutes one magnitude of brightness. The square-root of *N* represents the standard deviation from this one-magnitude's worth number of counts. As performed by many professional astronomers, all images in this project were assumed to have 3σ error in the measurements. The error bars were useful for showing the quality of a certain night's observations.

Typical extinction curves would have slopes of no greater than 0.15 magnitudes per airmass, positive or negative (Whiteley 2001). Figures 2-7 are the extinction curves for the KPNO infrared telescope. Each extinction curve represents a combination of the observations of all standard stars for that night.

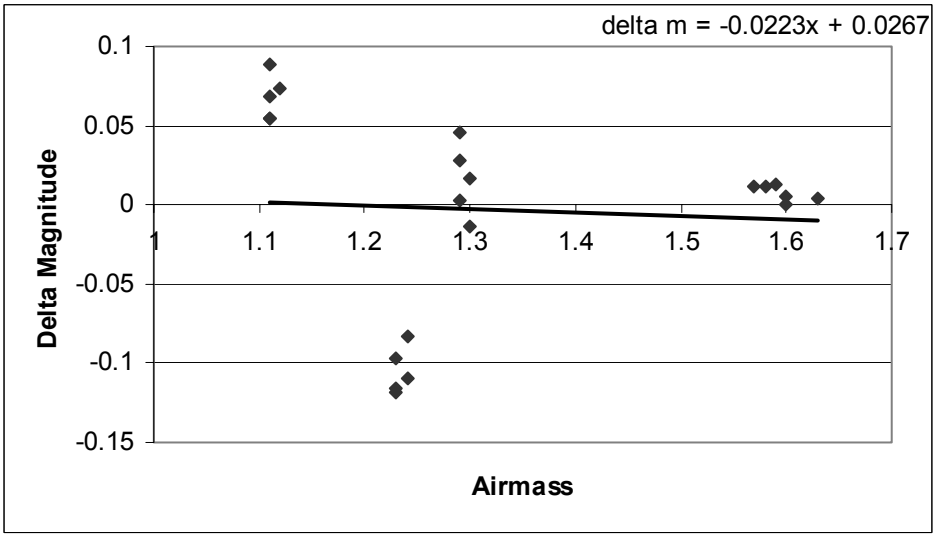

Figure 2. September 17 Extinction Curve, KPNO Telescope, J-Band

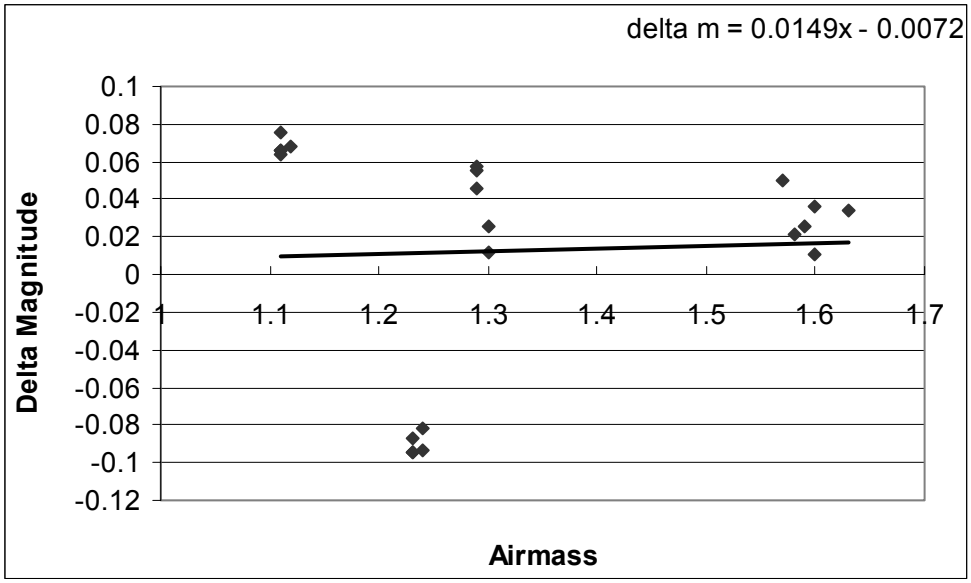

Figure 3. September 17 KPNO Extinction Curve, H-Band

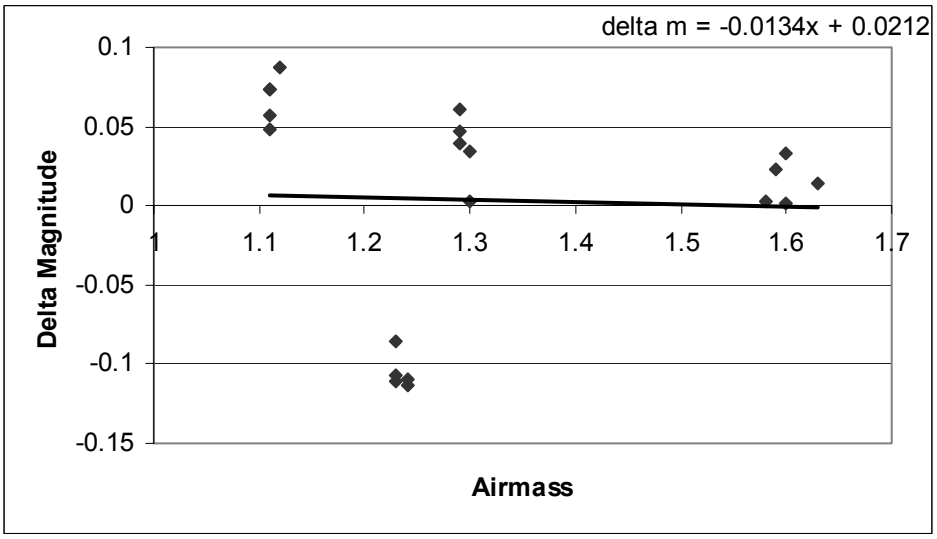

Figure 4. September 17 KPNO Extinction Curve, K-Band

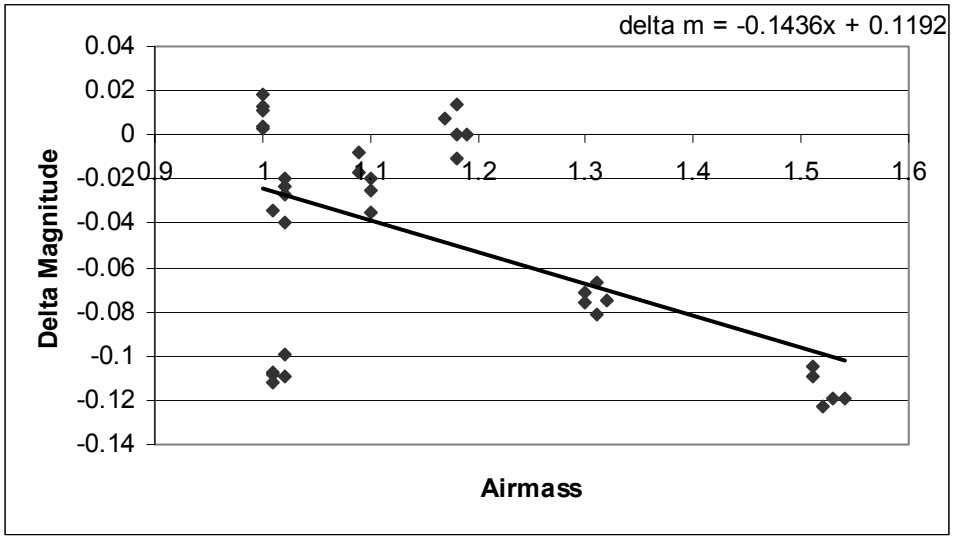

Figure 5. September 19 KPNO Extinction Curve, J-Band

While the extinction curve for the H-band on September 17 (Figure 3) had a slightly positive slope, the extinction curve for the H-band on September 19 (Figure 6) had a much sharper negative slope. September 19 had higher winds and consequently more noise in the atmosphere. Larger corrections would be needed, thus creating a larger slope on the extinction curve. Both curves come from the infrared telescope (KPNO).

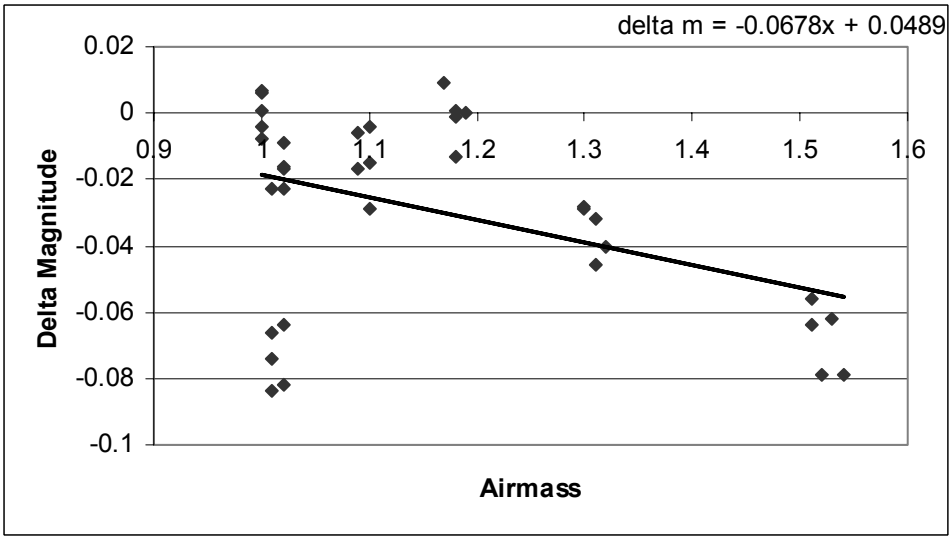

Figure 6. September 19 KPNO Extinction Curve, H-Band

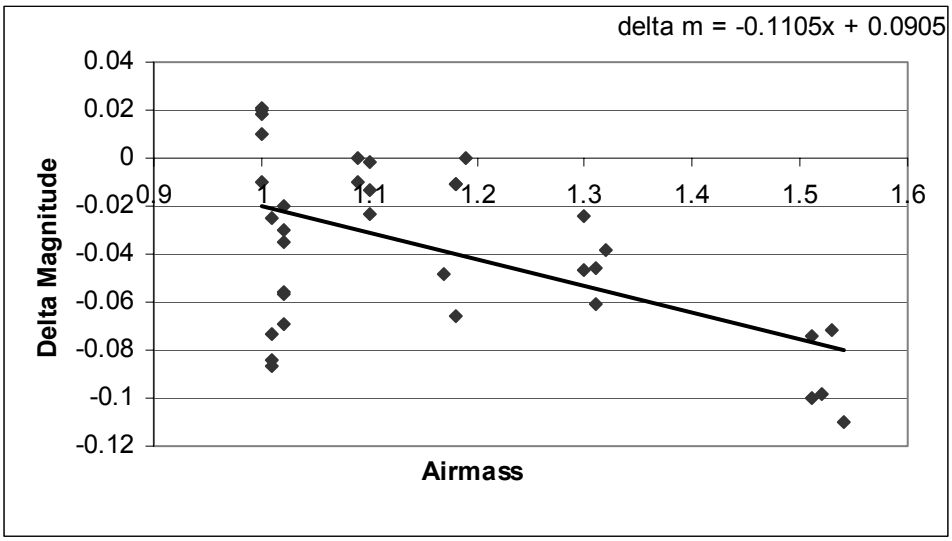

Figure 7. September 19 KPNO Extinction Curve, K-Band

Extinction curves were more similar within the same night as opposed to within the same filter. Each curve also had different extinction patterns between the infrared and optical filters, as seen between Figures 7 and 8.

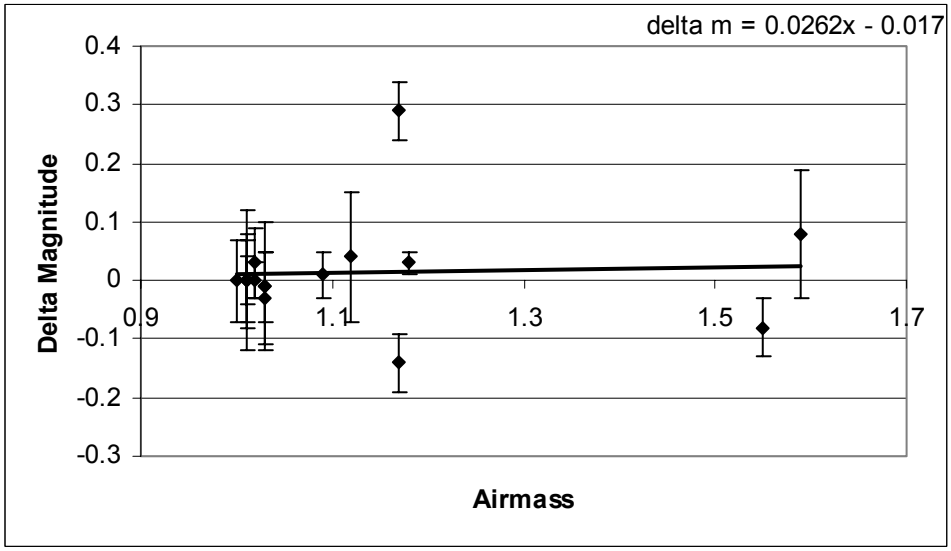

Figure 8. Steward Extinction Curve, V-Filter

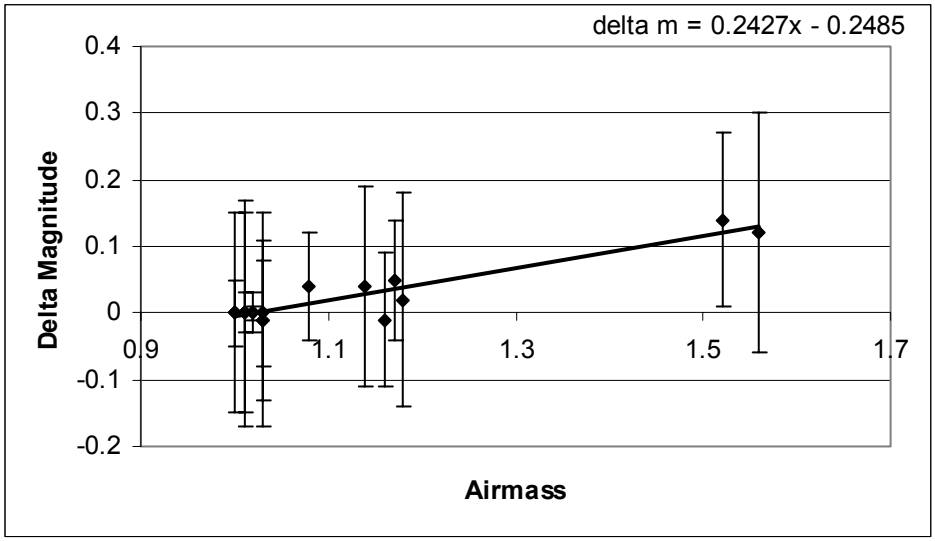

Figure 9. Steward Extinction Curve, B-Filter

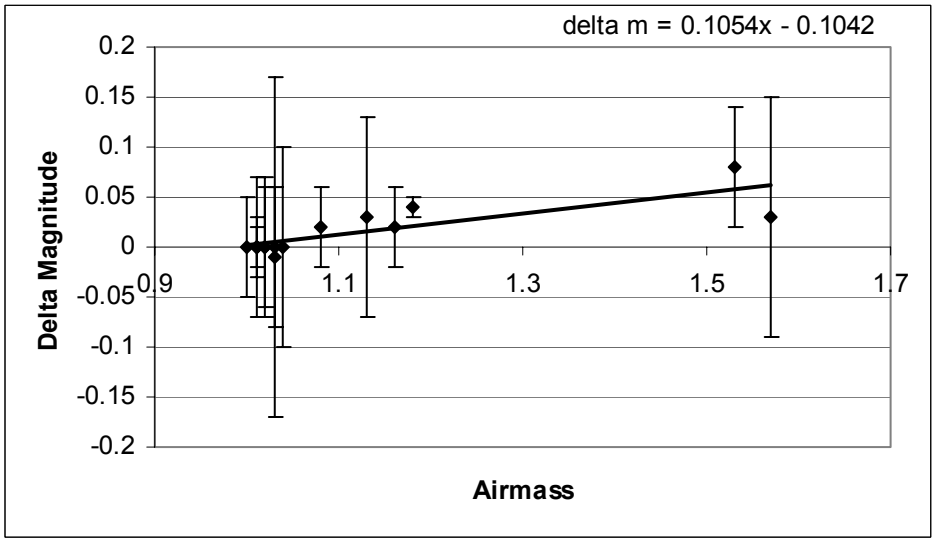

Figure 10. Steward Extinction Curve, R-Filter

The steeper extinction curve for the B-filter (Figure 9) than for the V-filter or R-filter (Figure 10) results because Earth's atmosphere scatters more light at bluer wavelengths. This is the same reason why the sky appears blue during the day.

Spacewatch also utilized an extinction curve, but for an unfiltered CCD. This extinction curve (Figures 11-13) accounted for light collected across all wavebands.

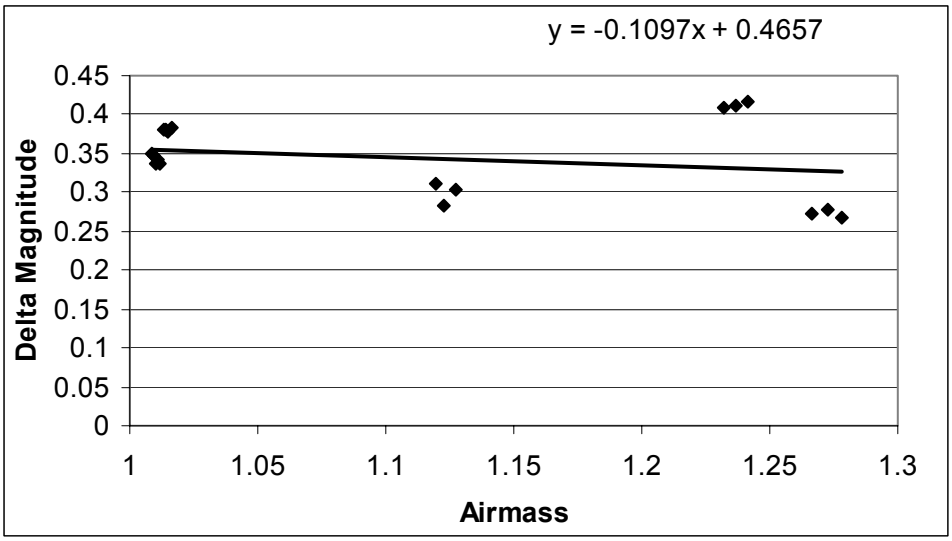

Figure 11. September 19 Spacewatch Extinction Curve

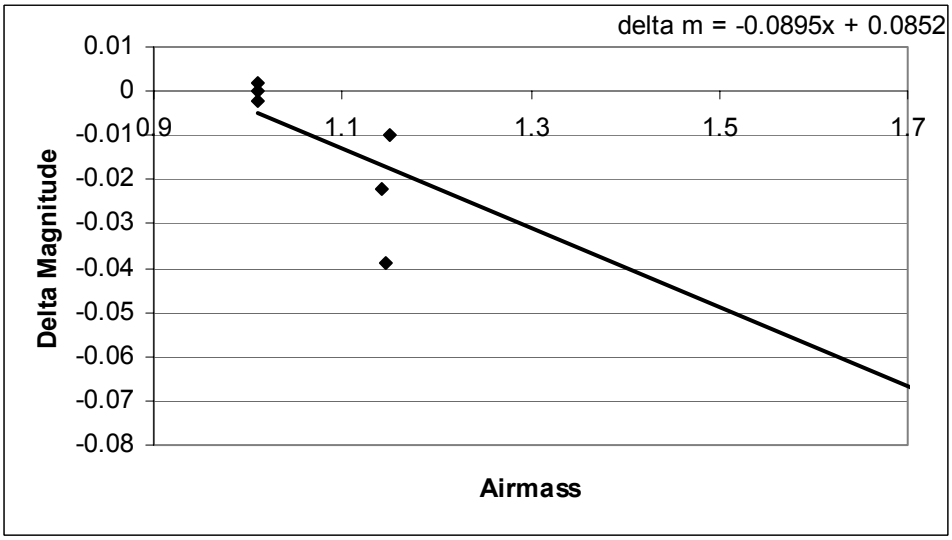

Figure 12. September 26 Spacewatch Extinction Curve

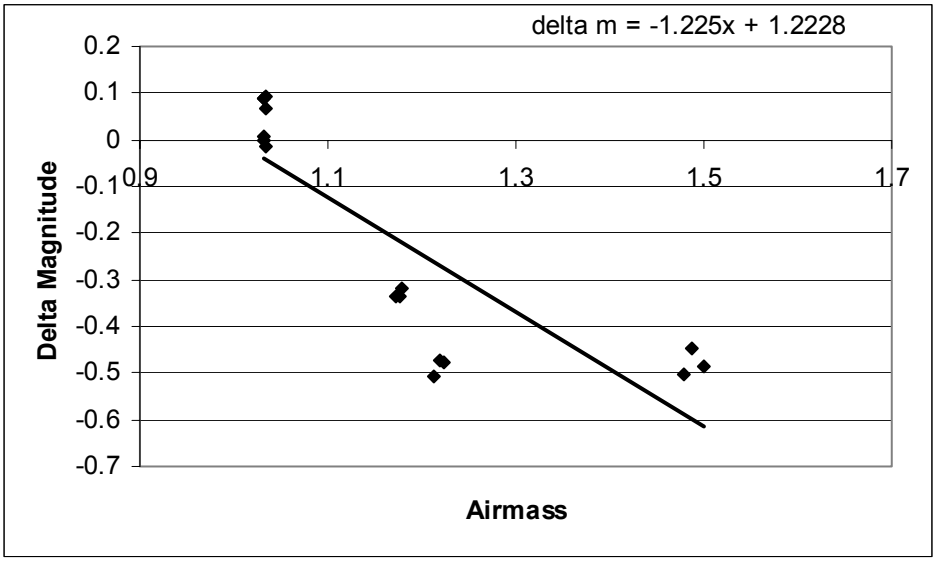

Figure 13. September 27 Spacewatch Extinction Curve

5. LIGHTCURVES

Lightcurves are plots of the relative brightness of an asteroid over time. Usually, lightcurves are observed from sunset to sunrise. Using these lightcurves, the rotation period and shape of the asteroid may be determined (Harris et al. 1989). The plot of the lightcurve will have a cyclical pattern to it, due to the complete rotation of the asteroid.

From composite lightcurves the general shape of the asteroid can be derived (Magnusson et al. 1988, Ostro et al. 1986, Michalowski 1993). The asteroid's lightcurve can be irregular due to the shape of the asteroid, due in part to a history of collisions. A study of the asteroid from different angles can yield the orientation of its rotation axis.

The shape[14] of the object can be estimated from the ratios of the lightcurve's maxima and minima. Generally, the brightness of the asteroid is proportional to the cross-sectional area of the object (Ostro 1986). This can be shown by the relation

$\frac{f_1}{f_2} = \frac{A_1}{A_2}$, where A is the cross-sectional area, and f is the calculated flux, both from the maximum and minimum of the lightcurve. Then

$$2.5 * \log(\frac{f_1}{f_2}) = 2.5 * \log(\frac{A_1}{A_2}) = (m_2 - m_1), \qquad \text{(Eq. 4)}$$

where m_2-m_1 corresponds to the difference between maximum and minimum magnitudes on the lightcurve. The ratio of the areas can be found from the amplitude of the curve.

The asteroid is initially assumed a triaxial ellipsoid. Each of the three axes is a different size. Production of a complete model of its shape would require observations from multiple ground-based locations. It has already been shown by Magnusson et al. that lightcurve data alone are not sufficient to determine the three-dimensional shape of the asteroid (1988). What can be approximated is a ratio of the broad side to the narrow side of the asteroid's shape.

Relationships between lightcurve shape and asteroid shape can offer insights into the type of asteroid (Burns & Tedesco 1979). Different taxonomic classes of asteroids are known to have certain lightcurve characteristics (range in magnitude, periods, etc.). These different classes, in turn, have been hypothesized to originate from different regions of the Solar System. Silicon and iron-based asteroids generally have larger amplitudes than carbon-based objects[15].

---

[14] This is assuming the asteroid to be an ellipsoid. Most asteroids discovered are triaxial ellipsoids (Ostro 1986).

[15] Tedesco and Zappala (1980) have found that, among a sample of 30 S-types and 26 C-types, the average amplitude of S-types is 0.193 +/-0.017 magnitude, while for C-types the average amplitude was 0.181 +/-0.024 magnitude. Binzel (1989) has found that the mean amplitude of Near-Earth Asteroids is larger than that for main-belt asteroids. This implies that Near-Earth Asteroids are more elongated and less spherical.

2002 HK12 2002 HK12 was the first object tracked on September 17 and has the best coverage in the sample. On succeeding nights, 2002 HK12 was tracked less frequently as the other members of the sample were introduced. It was nonetheless imperative that it still be tracked, for its period was unknown and could have been longer than the time spent on September 17. Calibration with the standard star removed atmospheric effects, which were minimal. Figures 14-16 are the lightcurves taken at different wavebands in the near-infrared on September 17.

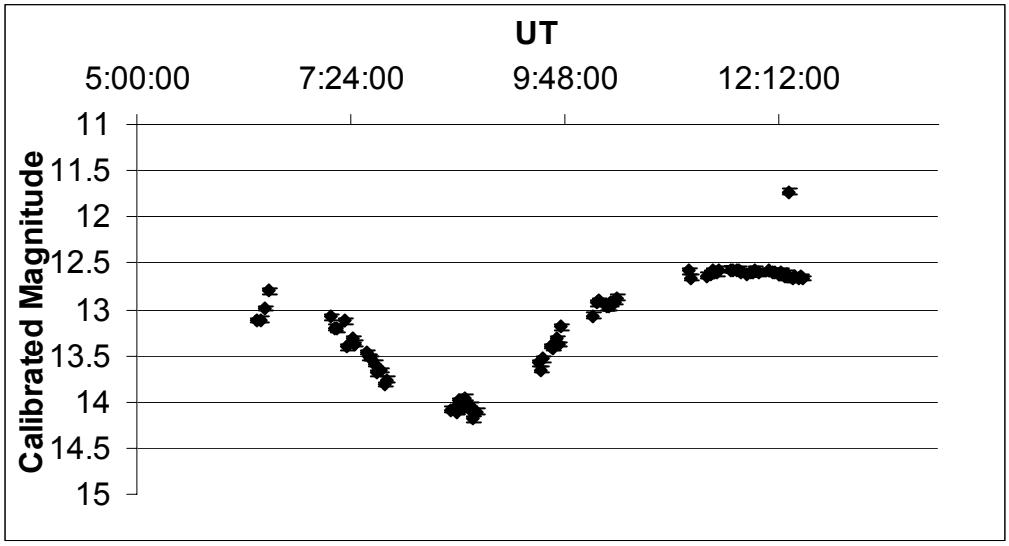

Figure 14. KPNO Lightcurve of 2002 HK12, J-Band September 17

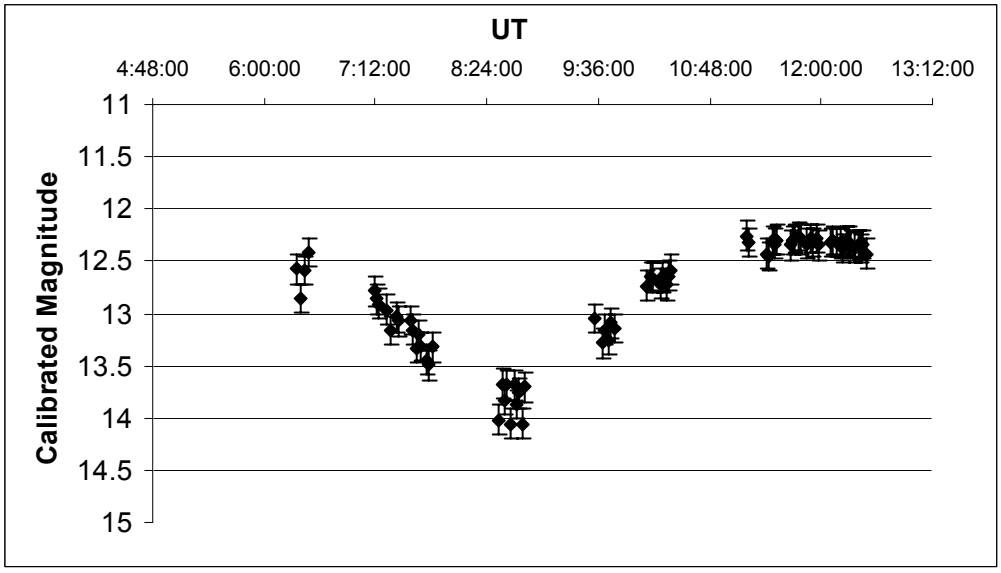

Figure 15. KPNO Lightcurve of 2002 HK12, H-Band September 17

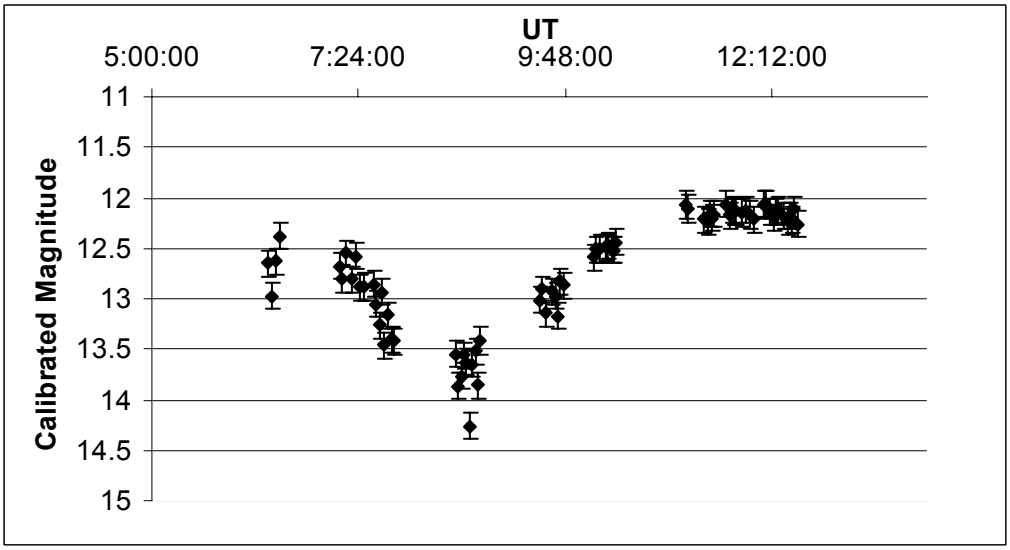

Figure 16. KPNO Lightcurve of 2002 HK12, K-Band September 17

All three wavebands in for September 17 produced similar lightcurves. On September 19, there were only a few observations made of 2002 HK12. With additional points a more complete curve might have been constructed for that night, but at the cost of observing the NEOs

2000 BF19 and 2002 KH3. 2002 HK12 was observed for approximately 30 minutes on September 19. These results are not shown here, but are part of the final analysis.

There were slightly differing magnitude ranges between the three wavebands for 2002 HK12. As for all objects, this is due to the object's color and albedo.

There was a characteristic dip in the brightness of 2002 HK12 on September 17 (Figure 17). This dip occurred around 0700-0730 UT. On the September 19 plot (Figure 18), it is evident that this dip initiates later in the night, at approximately 1100 UT.

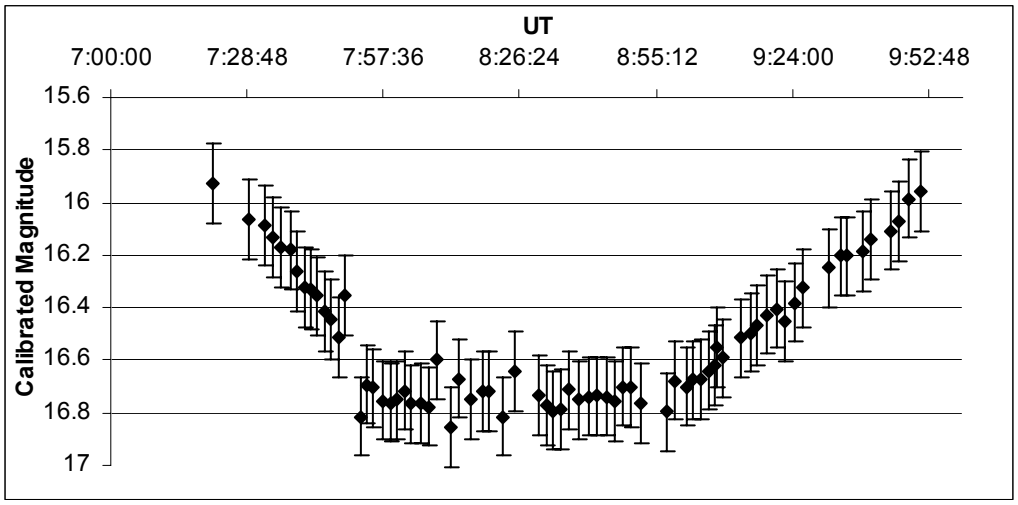

Figure 17. Spacewatch Lightcurve of 2002 HK12, September 17

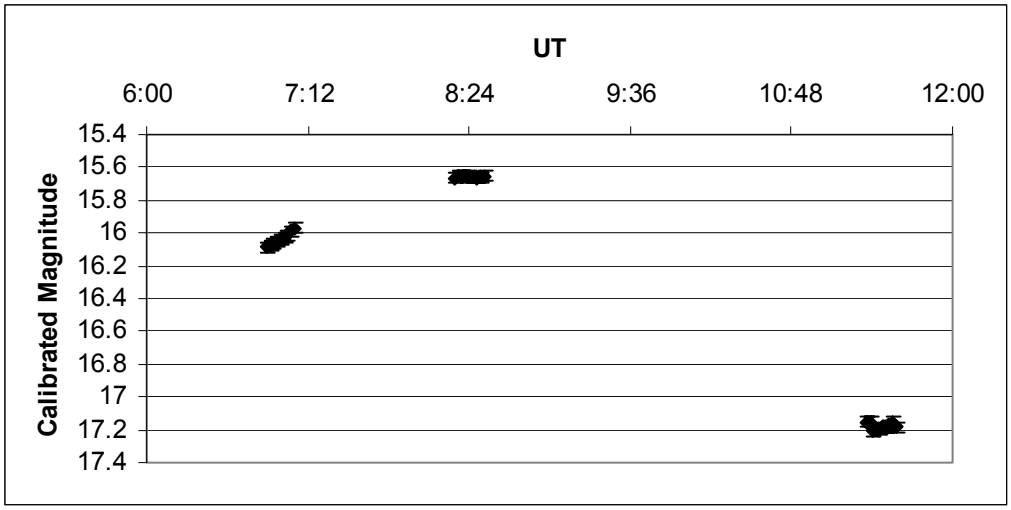

Figure 18. Spacewatch Lightcurve of 2002 HK12, September 19

2002 HK12 was the only one to have data from all four of the telescopes. The optical data gathered was much greater in quantity than the infrared, due to the competition to use the infrared imager. Spacewatch had taken simultaneous optical data on 2002 HK12 while infrared measurements were being made with KPNO on September 17 and September 19.

Similar to the procedure for KPNO, once a substantial amount of data was gathered on Spacewatch the first night, it was observed less often the second night to accommodate new candidates for investigation. Comparing images between KPNO and Spacewatch for September 17 and September 19 revealed that there were a larger number of images taken from the Spacewatch telescope. KPNO's dithering system would take up to 10 minutes for each set of infrared images, while Spacewatch could take images much more quickly during the night.

Both KPNO and Spacewatch provided evidence of the periodic and smooth change of 2002 HK12's brightness, which made further lightcurve analysis more successful.

Super-LOTIS was used to measure 2002 HK12 (Figures 19-20) on subsequent nights in the observing run. The Super-LOTIS lightcurve was unfortunately rougher due to its poorer resolution.

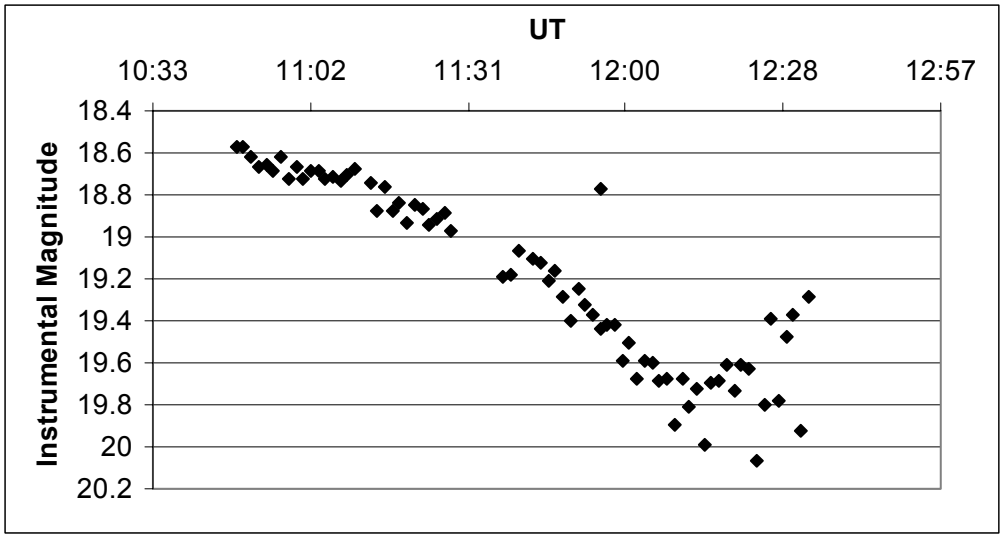

Figure 19. Super-LOTIS Lightcurve of 2002 HK12, September 20

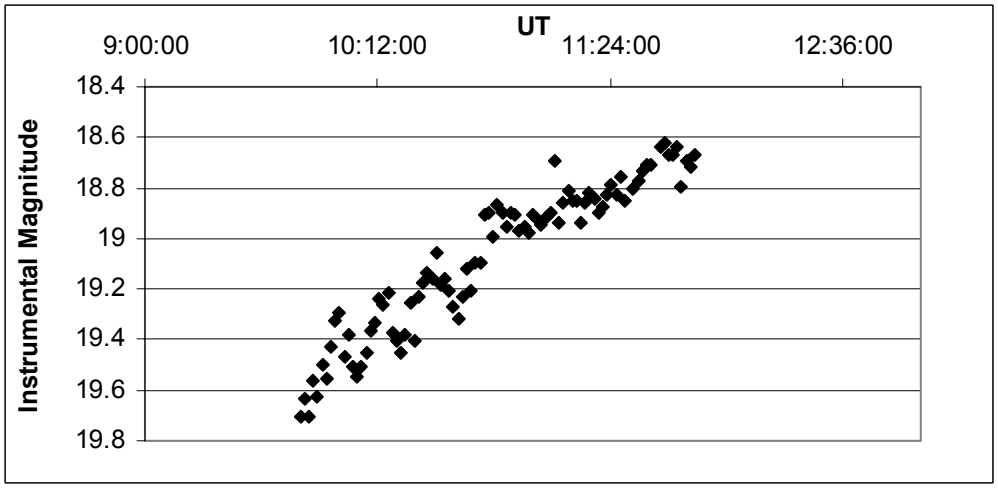

Figure 20. Super-LOTIS Lightcurve of 2002 HK12, September 22

Within the steadily decreasing magnitude of 2002 HK12 in the Super-LOTIS lightcurve, there is a very detectable periodicity. Additional lightcurve work was completed on 2002 HK12 using Spacewatch on the last couple of nights of the observing run (Figures 21-22).

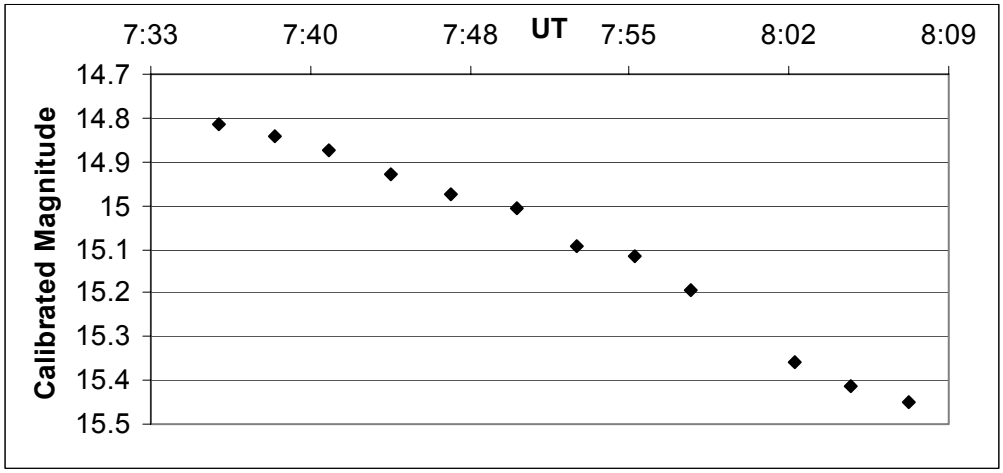

Figure 21. Spacewatch Lightcurve of 2002 HK12, September 26

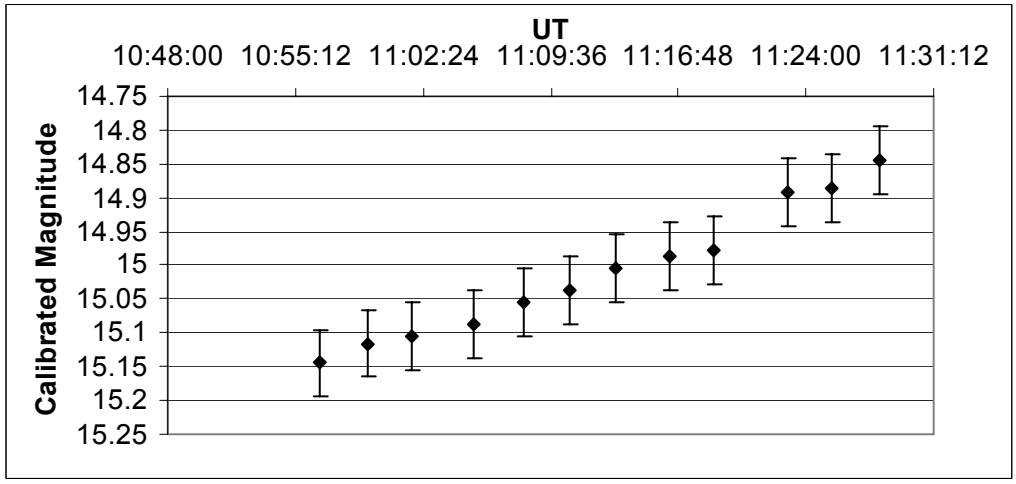

Figure 22. Spacewatch Lightcurve of 2002 HK12, September 27

2000 BF19 Like 2002 HK12, 2000 BF19 was observed with KPNO, Spacewatch and Steward (Figures 23-28). This NEO was farther from Earth than 2002 HK12. Its lightcurves are not as smooth as 2002 HK12 and the analysis of these curves was somewhat more difficult.

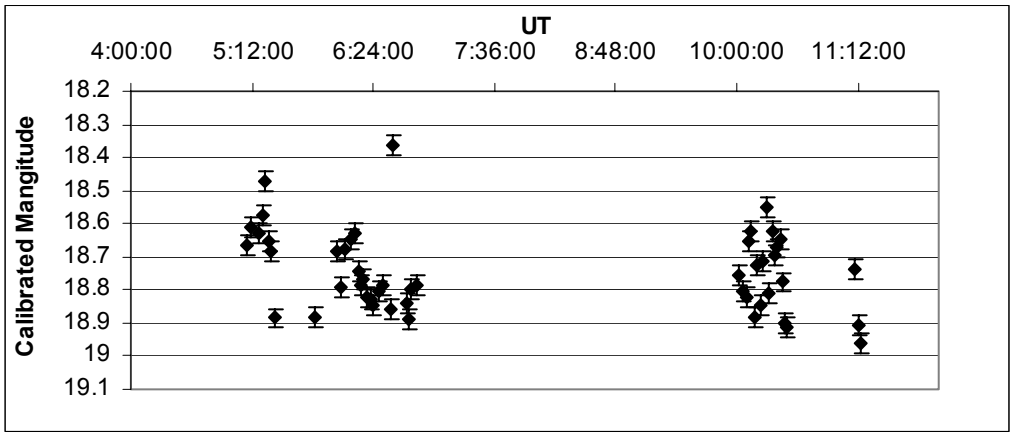

Figure 23. Spacewatch Lightcurve of 2000 BF19 on September 19

In addition, it is obvious from Figure 23 and 24 that there were gaps in the Spacewatch coverage. This is the result of allocating multiple objects to one night. Because of these gaps, it was more difficult to fit the lightcurve of 2000 BF19. September 27 had too few points for presentation here; however, it was used later in the lightcurve analysis.

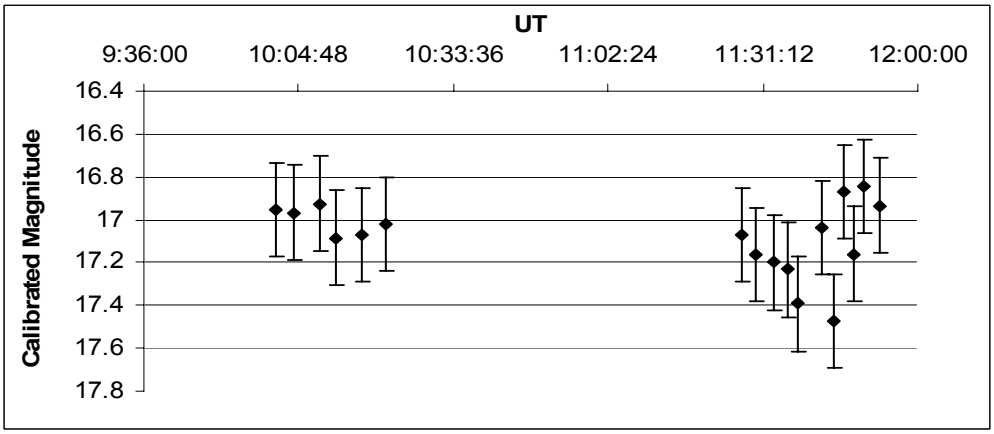

Figure 24. Spacewatch Lightcurve for 2000 BF19 on September 26

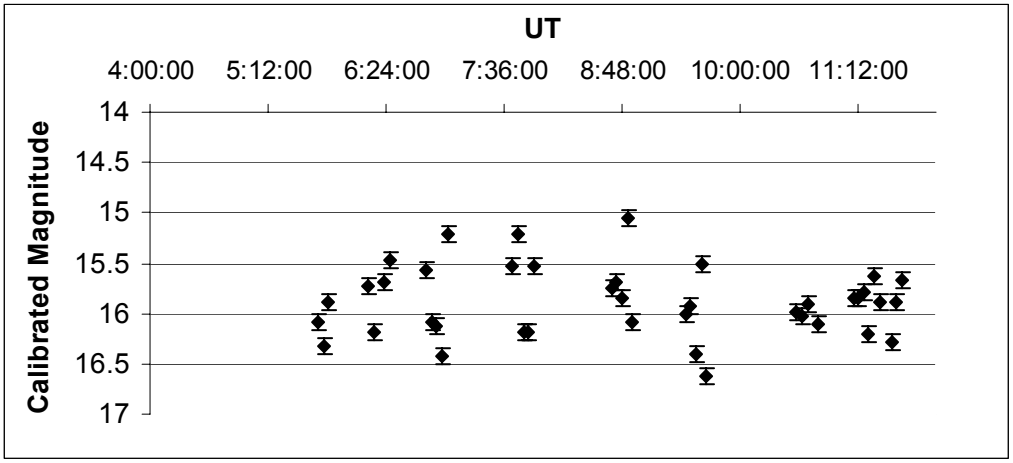

25.a)

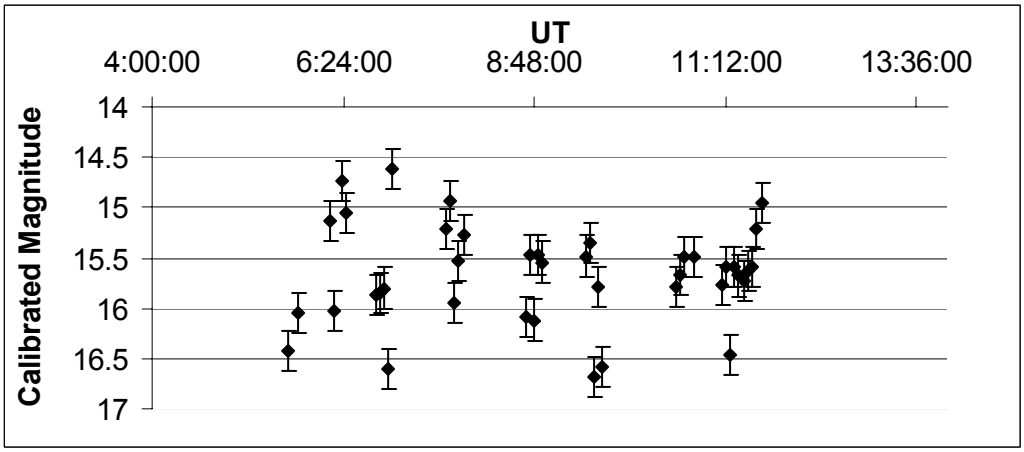

25.b)

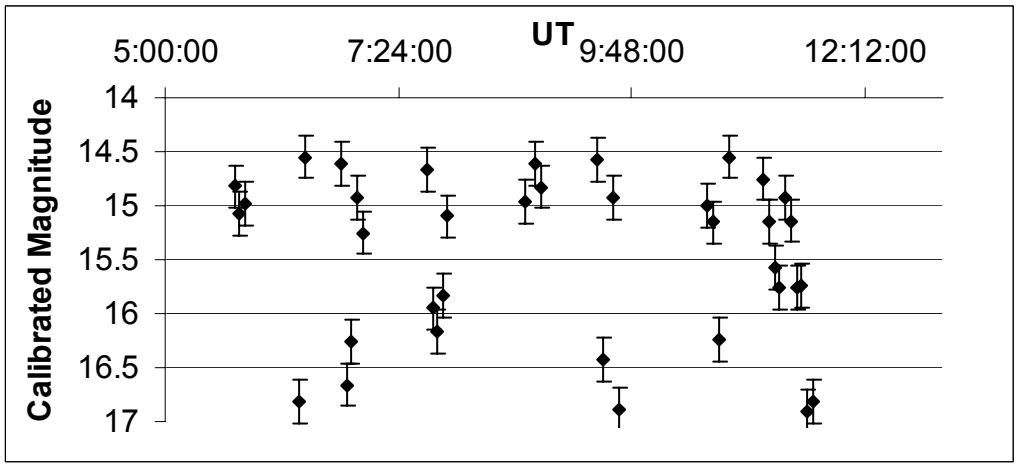

25.c)

Figure 25. a) J-Band, b) H-Band, c) K-Band lightcurves for 2000 BF19 from KPNO, Sept. 19

Figure 25 shows infrared measurements made for 2000 BF19 on September 19. As is evident across the three infrared wavebands, as the wavelength increases, the uncertainty in the measurements increases dramatically. It was very difficult to discern any periodicity in the K-band lightcurve for September 19.

Steward was used to produce V-filter lightcurves (Figures 26-28). The R and B filters were used for color measurements only. These V-filter lightcurves are more stable and consistent than the Spacewatch lightcurves (Figures 23 and 24).

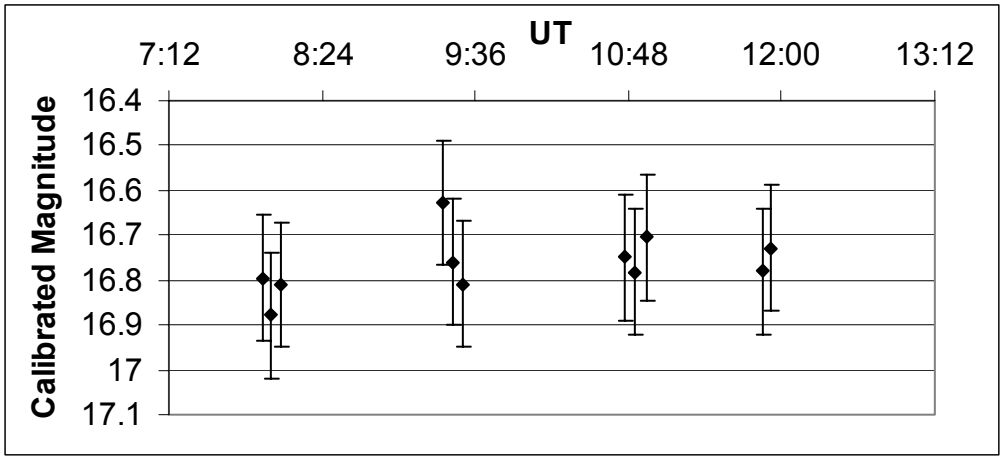

Figure 26. Steward Lightcurve for 2000 BF19 on September 20

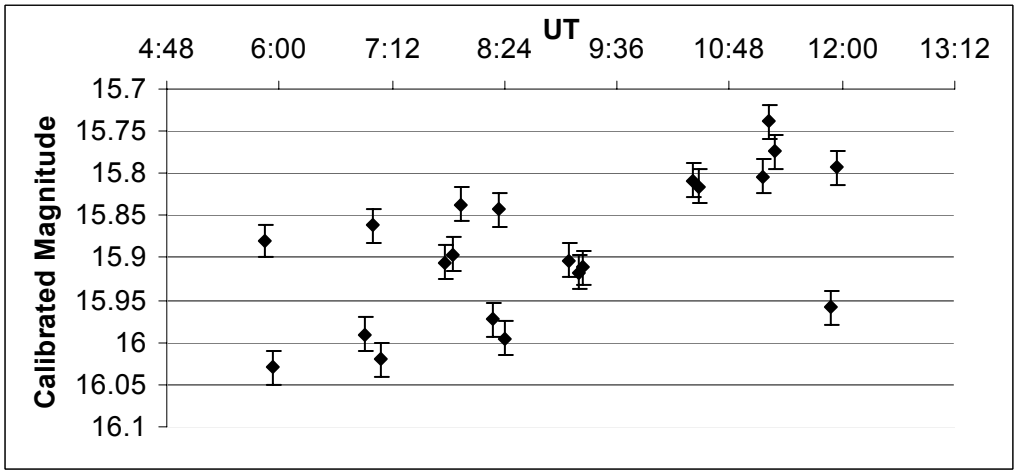

Figure 27. Steward Lightcurve for 2000 BF19 on September 21

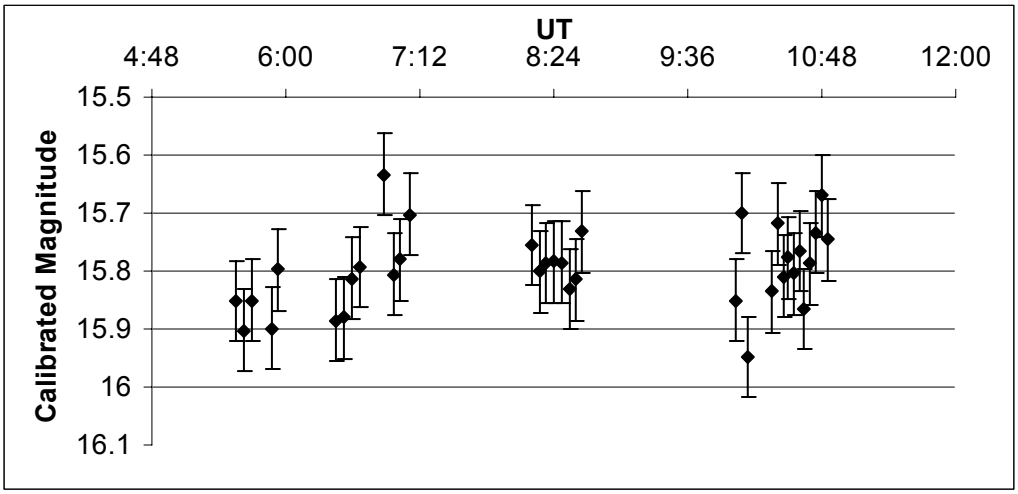

Figure 28. Steward Lightcurve for 2000 BF19 on September 22

2002 KH3 2002 KH3 like 2000 BF19 was first observed on September19, and is the third of three asteroids that had been observed both in the infrared and optical wavebands. The infrared lightcurves for 2002 KH3 appear in Figure 29; the optical lightcurves are shown in Figures 30-35. The KPNO observations made of 2002 KH3 reveal sporadic behavior amongst the J,H and K filters.

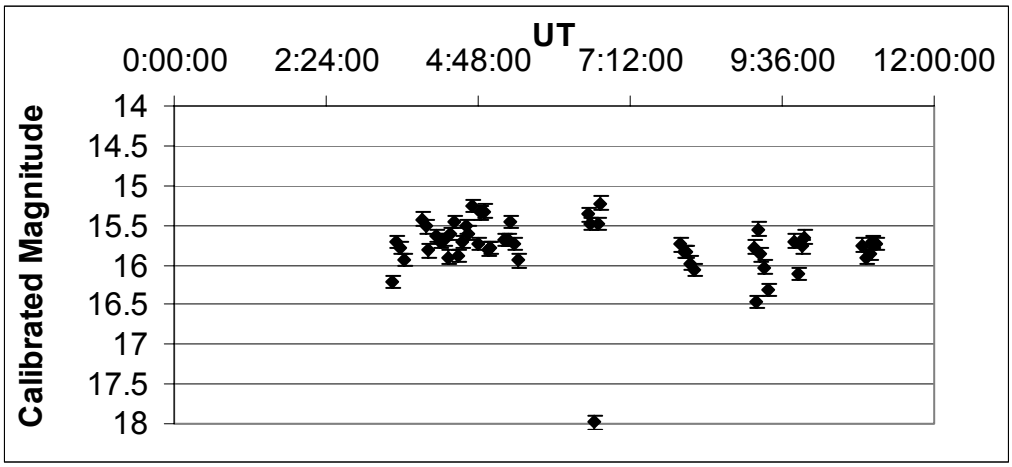
UT
0:00:00
2:24:00
4:48:00
7:12:00
9:36:00
12:00:00
Calibrated Magnitude
14
14.5
15
15.5
16
16.5
17
17.5
18

29.a)

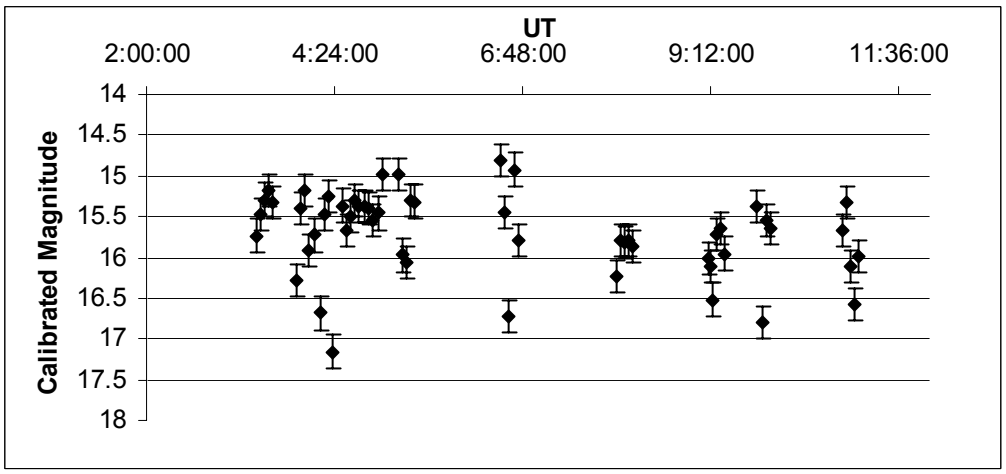
UT
2:00:00
4:24:00
6:48:00
9:12:00
11:36:00
Calibrated Magnitude
14
14.5
15
15.5
16
16.5
17
17.5
18

29.b)

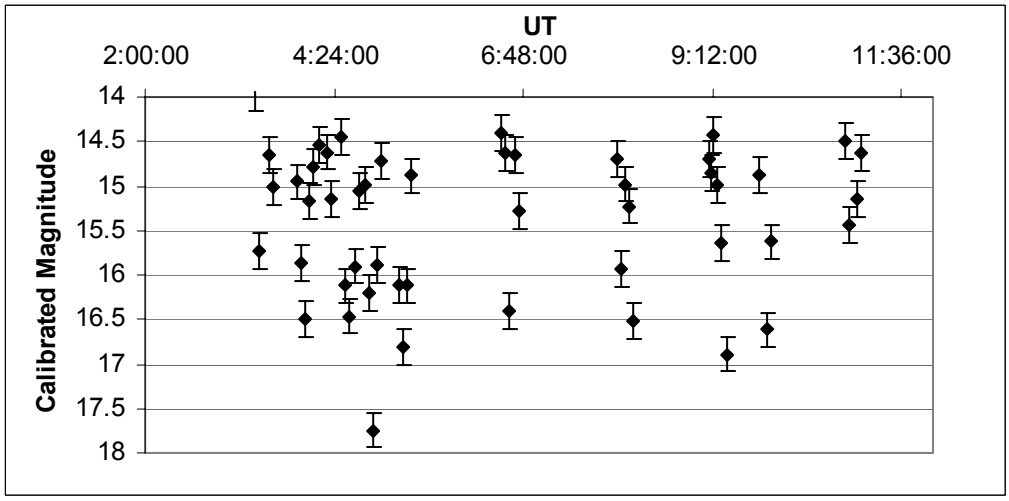
UT
2:00:00
4:24:00
6:48:00
9:12:00
11:36:00
Calibrated Magnitude
14
14.5
15
15.5
16
16.5
17
17.5
18

29.c)

Figure 29. September 19 KPNO curves for 2002 KH3: a) J-Band, b) H-Band, and c) K-Band.

In general, turbulent atmosphere can increase the thermal noise of an image. The random distribution of 2002 KH3's infrared curves was most probably due to the windy weather on September 19. Such winds could easily change the thermal emission being viewed by the camera. This changing thermal activity increased the noise collected by the imager. Further observation would be required to create an infrared lightcurve of 2002 KH3.

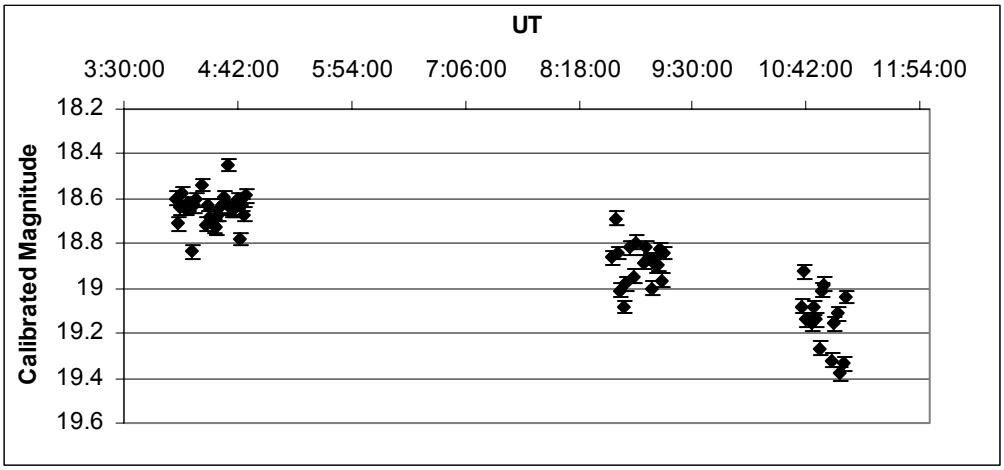

Figure 30. Spacewatch Lightcurve for 2002 KH3 on September 19

Steward Observatory's lightcurves (Figures 31-33) for 2002 KH3 on September 20, September 21 and September 22 are stable and do not show any random deviations or notable spikes. The consistent sampling over time of these objects was also beneficial, in contrast with the Spacewatch sampling pattern.

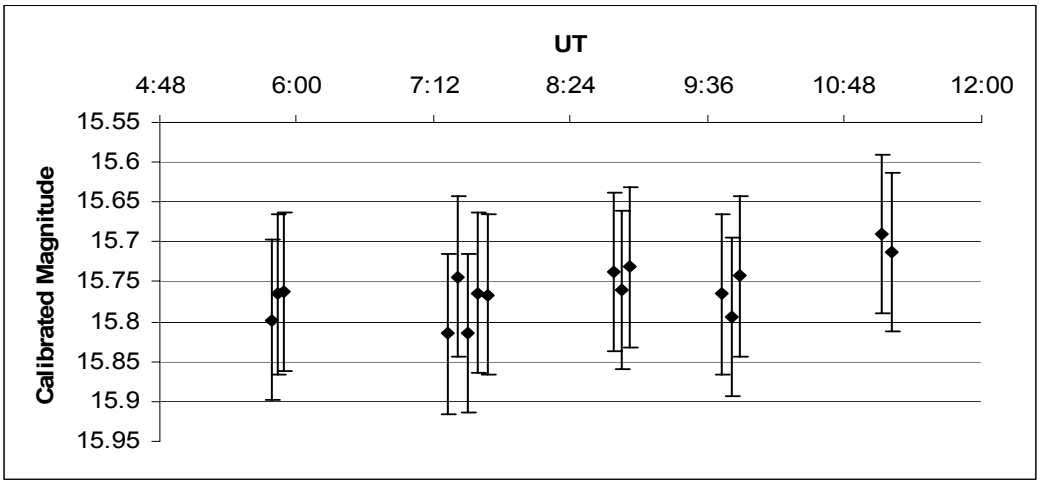

Figure 31. Steward Lightcurve for 2002 KH3 on September 20

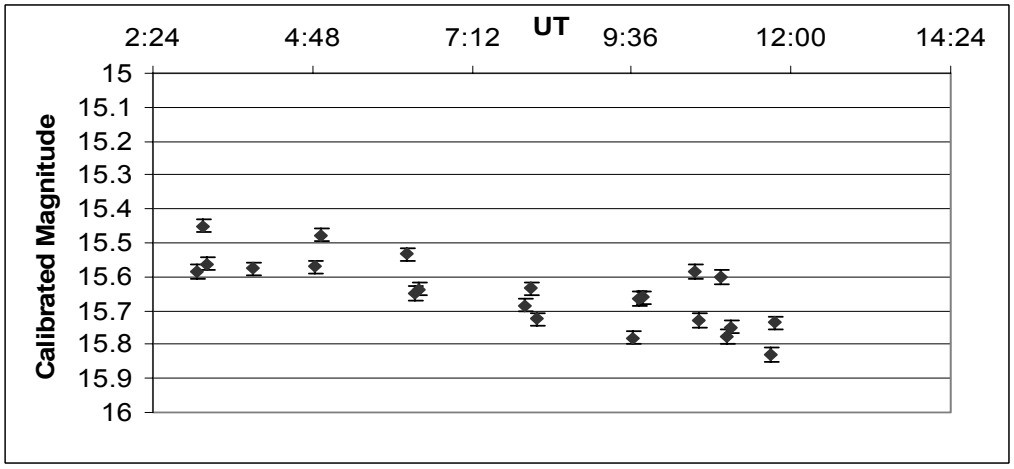

Figure 32. Steward Lightcurve for 2002 KH3 on September 21

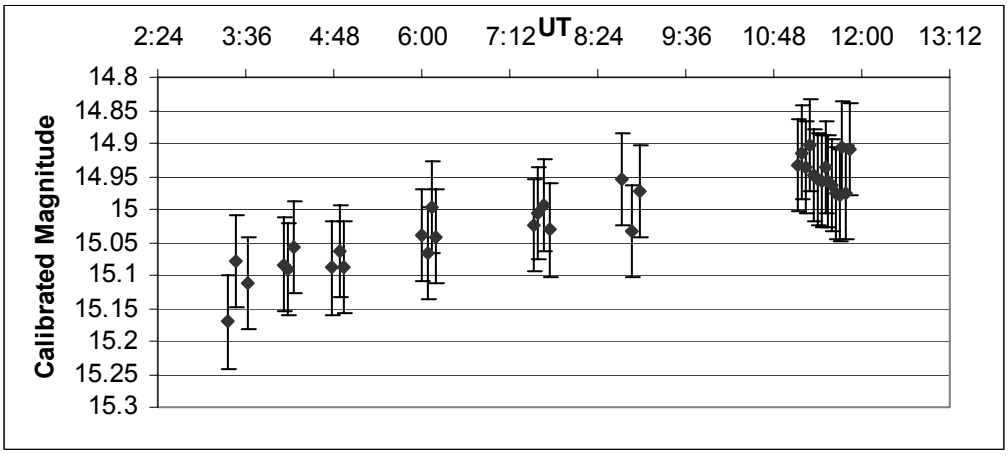

Figure 33. Steward Lightcurve for 2002 KH3 on September 22

The data points in Figures 31-33 from Steward are all smooth and continuous. They depicted a trend indicative of a periodic lightcurve, with only one or two deviations. September 26 in Figure 34 was very poor due to under-sampling. September 27 shows a smoother trend in the data.

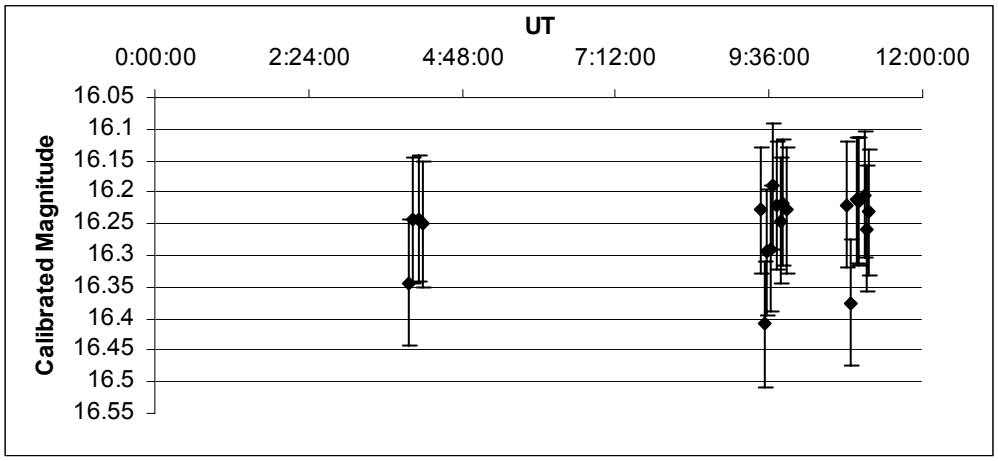

Figure 34. Spacewatch Lightcurve of 2002 KH3 on September 26

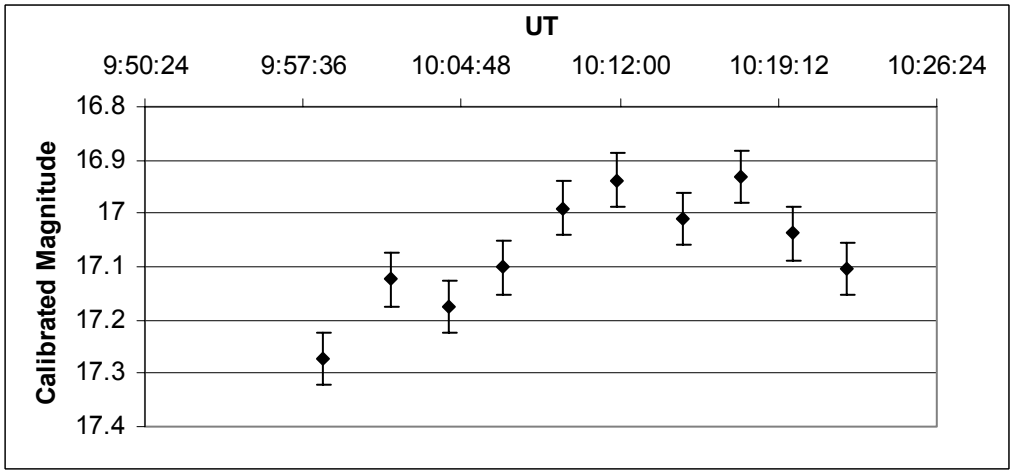

Figure 35. Spacewatch Lightcurve of 2002 KH3 on September 27

2002 PY39 Steward Observatory had a CCD that was able to narrowly focus in on its sources, and due to this strength a faint candidate, 2002 PY39, was chosen. 2002 PY39 was particularly hard to analyze because of its fast proper motion of 8.9 arcsec/minute in a northeasterly direction on the CCD. It was difficult to keep it from streaking on the image. However, by keeping the radius of aperture large enough, it was possible to perform photometry on it.

The aperture photometry performed here was especially meticulous so that no nearby stars were included in the measurement. There was an additional challenge since 2002 PY39 was passing through a dense star field each night. Some images had to be ignored. This asteroid was chosen due to its faint absolute magnitude. Its close position to Earth during the observing run made it especially measurable compared to its normally faint and distant position throughout the rest of the year. The optical lightcurves are shown in Figure 36.

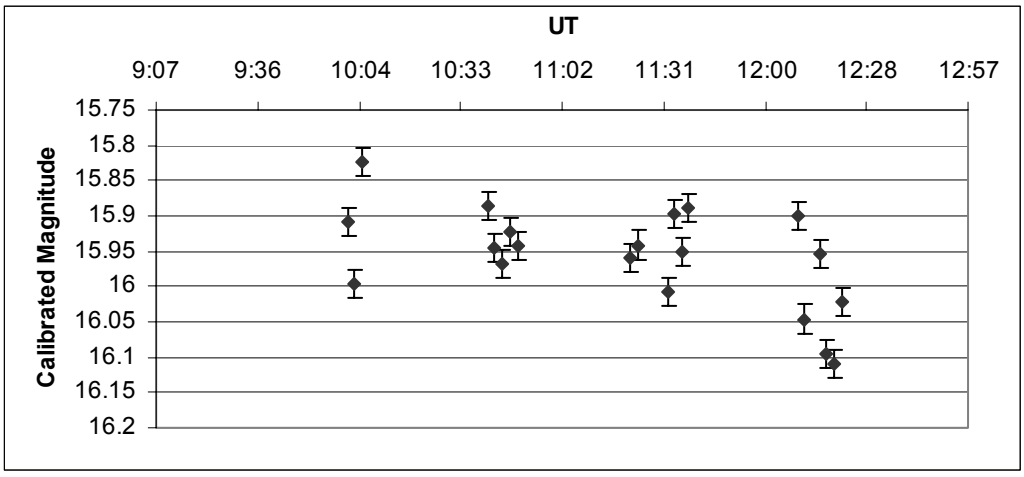

36.a)

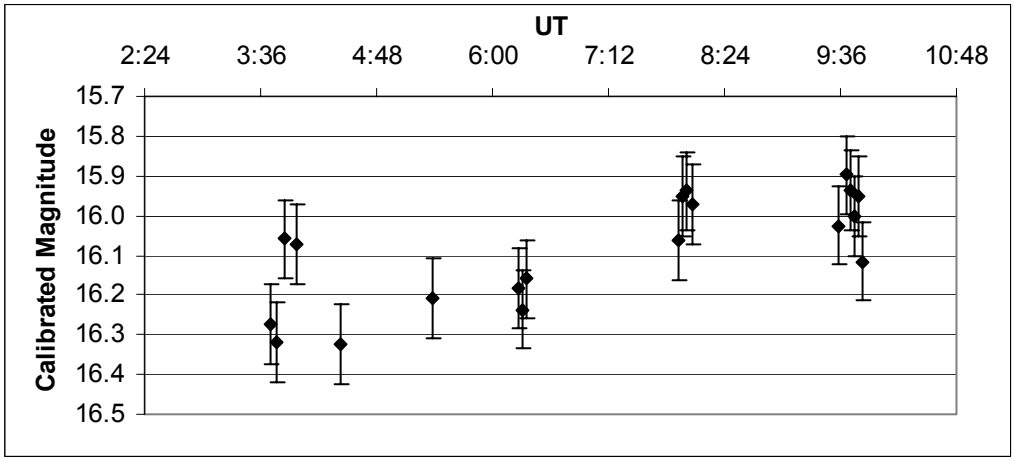

36.b)

Figure 36. Steward Lightcurves of 2002 PY39 on a) September 21 and b) September 22

6. ALBEDO

Albedo (*A*) is a measure of an object's reflectivity. The albedo calculated in this project aided in the taxonomic classification of the object and therefore the determination of its rough composition.[16] Different materials have different reflectivity. For example, metallic objects will reflect light more readily than non-metallic objects.[17] It is known that between S-type and C-type asteroids, S-type (the majority of NEOs) have an average higher albedo than C-type asteroids (Cunningham 1988).

Albedo is defined as the ratio of the reflected light to the incident light from the Sun. Sunlight is absorbed by the object and heats it. The fraction of absorbed light is $1 - A$. The absorbed light is re-emitted in the mid-infrared part of the spectrum (e.g., Fernandez et al. 2001).

[16] C-types have low albedo (0.065), S-types have moderate albedo (0.09-0.024), M-types have moderate albedo (0.07-0.21), Q-types have high albedo (0.21), D-types have low albedo (0.05), and E-types have high albedo (over 0.23) (Cunningham 1988). For this project the majority of asteroids will be of S and C-types.

[17] Some objects are now conjectured to be cometary in origin that have low albedos and contain water ice and organic compounds. These low-albedo objects could also be indicative of the primitive D-type asteroids, which are the most primitive (and thus best preserved) in the Solar System (e.g., DiMartino et al. 1997; Fernandez et al. 2001; Lazzarin et al. 1997). Other similar classifications of asteroids based on albedo can also be made.

The reflected visible light and the re-emitted infrared radiation are related to the object's albedo (*A)*:

$$f_{vis}/f_{IR} = A/(1 - A).$$

Rearranging terms,

$$A = \frac{(f_{vis}/f_{IR})}{(1 + f_{vis}/f_{IR})} \qquad \text{(Eq. 5)}$$

where f_{vis} and f_{IR} refer to the fluxes due to the respective visible light reflected and the infrared flux re-emitted (e.g., Zeilik & Gregory 1998).[18] Consequently, by observing the reflected visible light and the re-emitted infrared radiation, the albedo can be measured.

The two telescopes utilized in this project for such calculations were the Spacewatch telescope (for the optical measurements) and KPNO (for infrared measurements). The main challenge to the process was that KPNO was only equipped to conduct near-infrared measurements. Most albedo calculations conducted by astronomers have been done with mid-infrared observations (Morbidelli et al. 2002). When traveling to Arizona one primary expectation was that the L-band imager on the KPNO camera would be able to take photometric data. L-band is much closer to the mid-infrared range than the J, H, or K bands. However, the farther out one observes into the infrared range, the easier it is for that filter to saturate from infrared emissions. Such emissions in this range can come simply from the walls of the telescope itself. Exposure times that were sufficient for the J, H and K bands would completely saturate the L-band detector. The KPNO camera was built for use on both the KPNO telescope and 4-meter telescope on Kitt Peak. Because the KPNO 2.1-meter telescope was awarded for

[18] Magnitude and flux are related by $m_{max} - m_{min} = 2.5\log(f_{min}/f_{max})$.

this project, the relative size of the telescope restricted the capabilities of the infrared imager. Consequently, the L-band detector was not useful during this observing run.

In order to maximize the infrared radiation measured, the K-band detector's data was utilized and compared with the unfiltered optical measurements from Spacewatch. The difference between the V-K of the Sun and the V-K of the asteroid would reveal a limited amount of re-emitted infrared radiation. The albedos calculated here (Table 8) are thus deemed lower limits to the actual values.

Using

$$(V-K)_{Sun} - (V-K)_{asteroid} = 2.5 * \log(1/A) \qquad \text{(Eq. 6)}$$

rough albedos were calculated.

NEO	Albedo
2002 HK12	0.083
2000 BF19	0.12
2002 KH3	0.071

Table 8. Albedo for 2002 HK12, 2000 BF19, and 2002 KH3

7. OPTICAL COLOR

The color of an NEO is also used to determine the taxonomic classification and chemical composition (Binzel 1989).[19] Objects high in iron content are known to be redder than those high in water ice content. Hydrocarbons and pure elemental carbon cause the object to look blue/white. Featureless objects (without any definitive color) may be too small to be distinguishable, or they may be extinct cometary nuclei, high in water ice content (Weissman et al. 1989).

[19] Cunningham (1988) states that asteroids should appear redder at maximum than at minimum Sun-reflection for amplitudes less than 0.03 magnitude. Most Near-Earth Asteroids are reddish S-types. E-types (relatives of the S-type) are colorless, being iron-free silicates.

Color indices aid in taxonomic analysis. A color index is the difference in measurement between two separate filtered measurements, such as B (blue) and V (green). B-V colors that have larger values indicate redder colors, and are representative of iron-based and silicon-based NEOs (also known as S-types). Low B-V colors are indicative of carbon-based NEOs (C-types). B-V colors are the most widely used for taxonomic classifications.

2002 HK12's color measurements were determined at Steward and KPNO. Averages of the measurements in the B, V, R, J, H and K filters (Table 9) were taken to determine the average color index of the object.

Filter	Magnitude
B	15.07+/- 0.03
V	13.88+/-0.04
R	13.52+/-0.05
J	12.79+/-0.02
H	12.54+/-0.04
K	12.42+/-0.06

Table 9. Colors for HK12.

Color measurements for the sample are in Tables 9, 11, 13, 15 and 17. Color indices were calculated (Tables 10, 12, 14, 16 and 18) that are unique to the chemical composition of a particular asteroid. From these color indices, taxonomic classifications can also be assigned to the asteroids. 2002 KH4 and 2002 PY39 did not have any near-infrared measurements because they were not observed with KPNO.

Color Indices	
B-V	1.12
V-R	0.35
J-H	0.25
H-K	0.12

Table 10. Color Indices for 2002 HK12.

Similar work was performed for 2000 BF19, 2002 HK12, 2002 KH4, and 2002 PY39.

Filter	Magnitude
B	17.91 +/- 0.03
V	16.68+/- 0.04
R	16.18+/-0.05
J	15.88+/-0.02
H	15.70+/-0.04
K	15.47+/-0.06

Table 11. Colors for 2000 BF19

Color Indices	
B-V	1.23
V-R	0.49
J-H	0.18
H-K	0.23

Table 12. Color Indices for 2000 BF19

Filter	Magnitude
B	16.67+/-0.03
V	15.67+/-0.04
R	15.21+/-0.05
J	15.78+/-0.02
H	15.41+/-0.04
K	15.47+/-0.06

Table 13. Colors for 2002 KH3

Color Indices	
B-V	1.07
V-R	0.47
J-H	0.36
H-K	0.03

Table 14. Color Indices for 2002 KH3

Filter	Magnitude
B	16.69+/-0.03
V	15.65+/-0.04
R	15.01+/-0.05

Table 15. Colors for 2002 PY39

Color Indices	
B-V	1.04
V-R	0.68

Table 16. Color Indices for 2002 PY39

Filter	Magnitude
B	18.22+/-0.03
V	17.81+/-0.04
R	17.74+/-0.05

Table 17. Colors for 2002 KH4

Color Indices	
B-V	0.41
V-R	0.07

Table 18. Color Indices for 2002 KH4

8. BROADBAND SPECTRA

Spectral measurements were conducted by individually measuring the magnitudes of light at different wavebands. Broadband observations of spectra can be very useful in constraining the composition or taxonomic class of the asteroid. Both filters and infrared imagers were used to measure the intensities at these different wavebands.

Bus et al. (2002) have indicated that the waveband centered on 700 nm is a critical area for taxonomic classification of asteroids. At this waveband is a maximum emission feature in the spectra of many classes of asteroids. The slope before and after this peak is characteristic of the NEO type, particularly in the optical wavebands. Quantitative comparisons with published curves such as Tholen's (1984) will also aid in classification.

Figure 37 displays the broadband spectra calculated from the color measurements of three of the members of the sample for which infrared data was taken. The BVR colors were then plotted (Figure 38) against published BVR slopes for a C-type NEA and an S-type NEA.[20] From this comparison, the taxonomic classification of the asteroid can be further constrained. In addition, the slope of the spectrum is used to determine the taxonomic class of the NEO (e.g., Lazzarin et al. 1995; Gaffey et al. 1989). Numeric slopes were also calculated for the initial line segment (known as the principal component) of the broadband curve for all five NEOs, as shown in Table 19.

NEO	Slope (mag/100nm)
2002 HK12	0.22
2000 BF19	0.28
2002 KH3	0.20
2002 PY39	0.27
2002 KH4	-0.14

Table 19. Slopes of NEO sample from principal components of broadband spectra

[20] This diagram displays the relative reflectivity (y-axis) of different taxonomic classes of asteroids over a range of wavelengths (from 200 to 1200 nm).

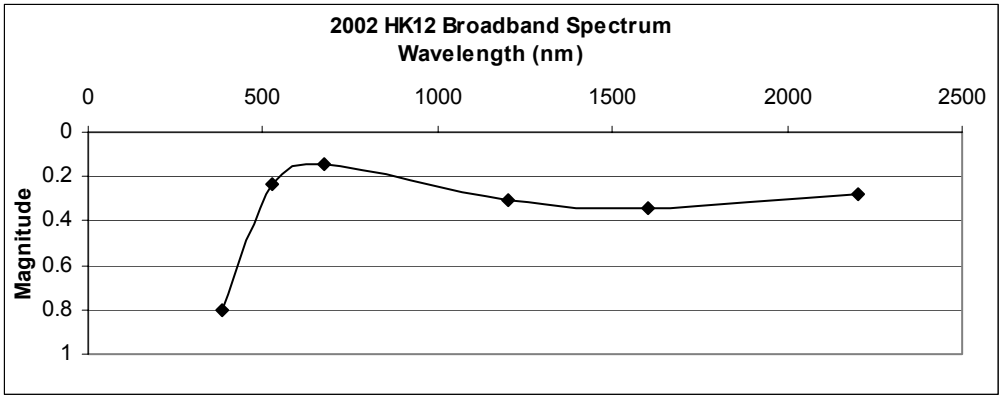

37.a)

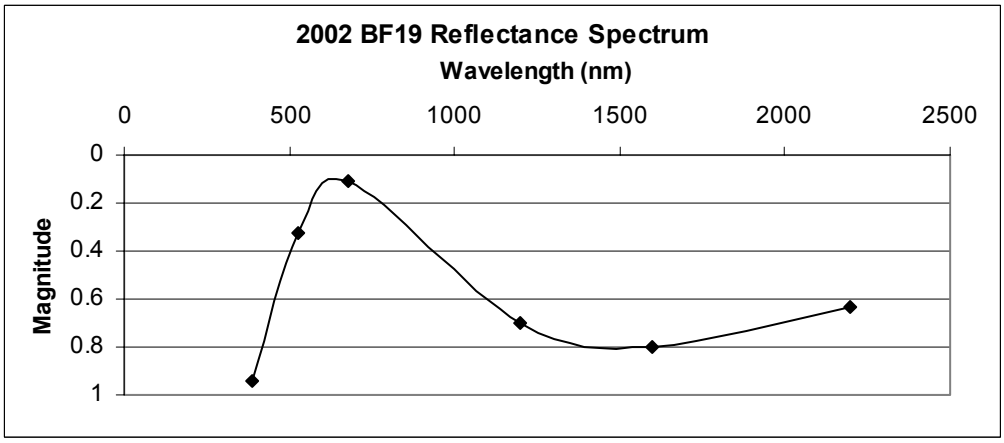

37.b)

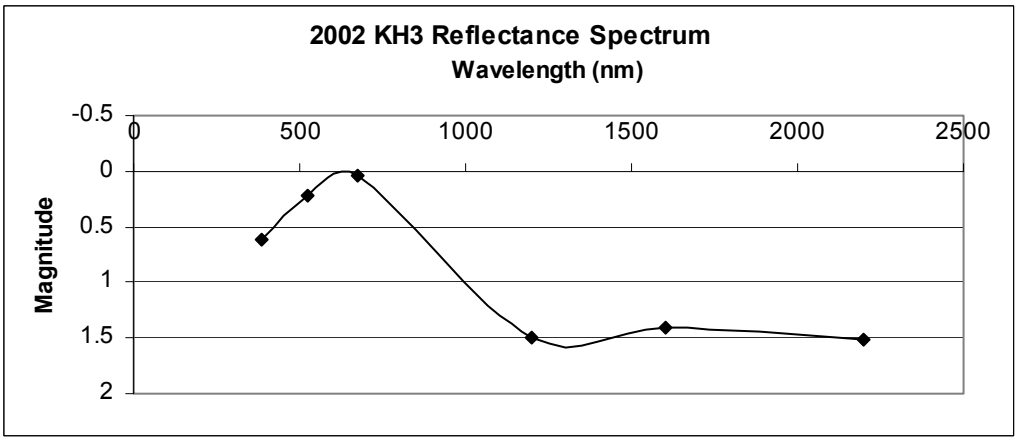

37.c)

Figure 37. Broadband Spectra of a) 2002 HK12, b) 2000 BF19, c) 2002 KH3

38.a)

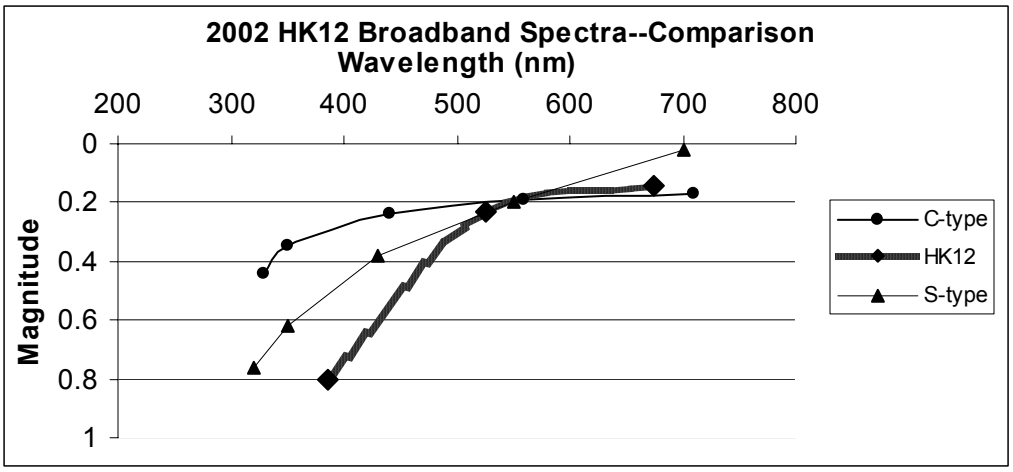

38.b)

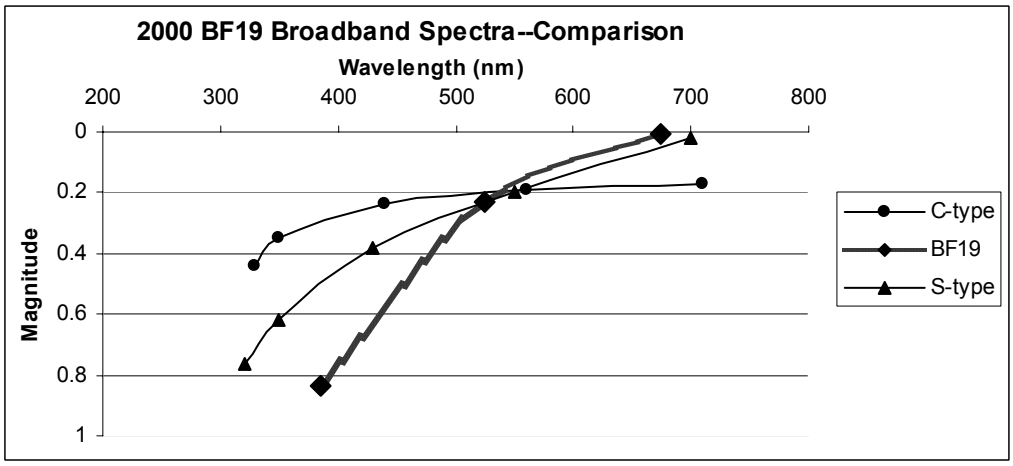

38.c)

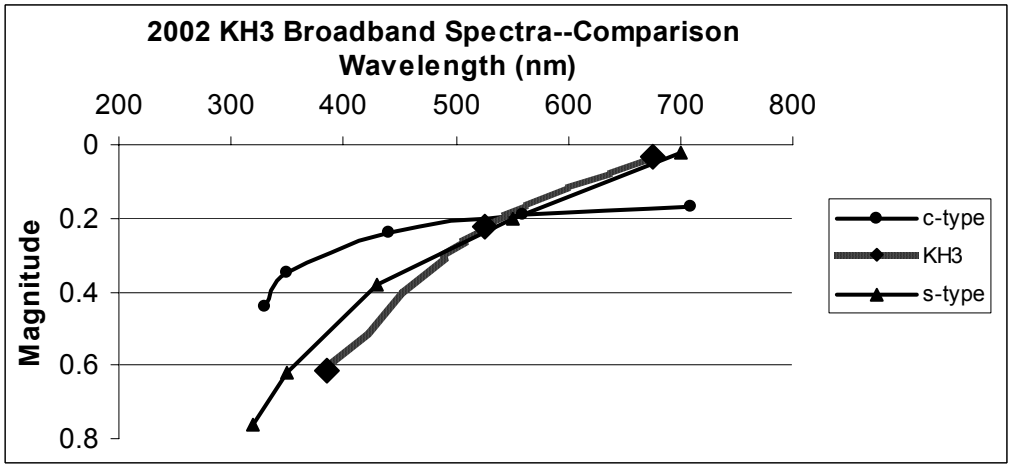

Figure 38 (a,b,c). Reflectance Spectra Comparisons with Tholen (1984b).

A steep slope usually indicates an object with metallic characteristics (closer to S-type), while a flat slope is indicative of a primitive object (C-type), full of elemental carbon and hydrocarbons (Lazzarin et al. 1995).[21] A comet would also have a flat slope, due to its non-metallic consistency.

The slope is broken into "components." Each component is a straight-line segment of the curve. There are typically 2-3 different components per spectral slope, with the first and most important one called the "principal component". S-type asteroids usually have principal component slopes of 0.30-0.60 mag/100nm, while C-types have roughly negative 0.15 to positive 0.15 mag/100nm.

The spectra of the sample in Figure 38 showed similarities with Tholen's published slopes in the BVR (optical) regions. The optical region is the limit of his spectra and many other published spectra. By extending these measurements into the near-infrared, it is possible to achieve a more detailed level of comparison and classification (Bus et al. 2002). The near-infrared spectra qualitatively follow known S-type slopes in the optical spectrum.

The spectra for 2002 HK12, 2000 BF19 and 2002 KH3 in Figure 38 have sharp positive slopes in the BVR regions (400-700nm). All three also have slopes that are more gradual in the JHK wavebands, as shown in Figure 37. 2002 PY39 also had a steep BVR slope. 2002 KH4 had a curiously shallow negative slope. Both of these objects did not have any near-infrared data points for a more complete broadband spectrum. The spectral lines are fitted to the six data points from the six-color photometry of the project.

[21] Asteroids that are "primitive" are those that have hardly changed (from heating, melting, collisions, etc.) since the formation of the Solar System, and are thus prime candidates for studying the history of the formation of the Solar System (Lazzarin et al. 1995).

9. ANALYSIS & DISCUSSION

Table 20 gives a summary of the physical properties of Near-Earth asteroids, and how these properties can differ among the different taxonomic classes of asteroids. With multiple methods of analysis the taxonomic classification of the NEO sample can be constrained to a degree of higher confidence than if there were only one or two methods of analysis.

Elements	Type	B-V index	Albedo	Spectral Slope	J-H/H-K indices
Carbon	C	0.6-0.8	0.04-0.06	-0.15—0.15	0.45/0.05
Silicon	S	0.8-1.3	0.09—0.24	0.30-0.60	0.35/0.06
Metals	M	0.7-0.9	0.07-0.21	Varied	0.42/0.05

Table 20. Near-Earth Asteroids and their physical properties.[22]

The optical and infrared characteristics of each NEO are inter-related. For example, the B-V index of the S-type is red, while its J-H index is lower. Consequently, the visual reflectance is higher than the thermal emission from heating. The opposite is true for those whose visual reflectance is low and infrared emission is high. From this table one could infer that the more iron or metal-based an object is, the higher the B-V index and lower J-H or H-K indices (Veeder et al. 1983). One could also infer that that the more carbonaceous or hydrocarbon-based an object is, the lower the B-V index and lower the J-H/H-K indices.

2002 HK12 2002 HK12 was discovered on April 30, 2002, by the Jet Propulsion Laboratory Near-Earth Asteroid Tracking Program in Pasadena, California. Its solar elongation[23] was an

[22] Physical Properties referenced from Binzel et al. 2001, Bus et al. 2002, Cunningham 1988, Dahlgren et al. 1997, Lazzarin et al. 2001, Leake et al. 1978, Veeder et al. 1983, Vilas et al. 1993, Wisniewski et al. 1996.

average of 130 degrees from September 17-28, and its motion across the sky was 2.6"/min to the west, and 1.6"/min to the south. Its orbital classification is Amor.

The lightcurve analysis of 2002 HK12 and the other members of the sample was performed using a Fourier analysis to fit the lightcurves. The fit itself was done mathematically from a program developed by astronomer Alan W. Harris known as FALCFAZ. This analysis developed a more precise lightcurve from the initial calibrated data (see Appendix for strength parameters of Fourier fits). First, all the lightcurves were plotted on the same time axis. There were holes in this composite plot due to daytime hours. A period was estimated from this plot. The strongest frequency would correspond to the actual period of the asteroid. Uncertainty in the calculated period came from the quality of the Fourier fit.

Average periods of Near-Earth Asteroids are approximately 5-13 hours (Alfven 1964). From the initial lightcurves of 2002 HK12 the period was estimated to be 12 hours. This period was then put in the Fourier transform function given below,

$$V(t) = \sum_{n=1}^{k} A_n \sin\frac{2\pi n(t-t_o)}{P} + B_n \cos\frac{2\pi n(t-t_o)}{P}, \qquad \text{(Eq. 7)}$$

where $V(t)$ is the magnitude calculated from the Fourier transform, P is the estimated period, t-t_o is the time interval (in this case the entire observing run), and A_n and B_n are the amplitude constants that determine the strength of the estimated period. The variable n reflects the order, or harmonic, of analysis being performed. The analysis becomes more refined for higher orders of n, but only works for NEOs with enough coverage.

---

[23] "Solar Elongation" refers to the angular separation between the object and the Sun, with respect to an observer on Earth. If the object were to be situated directly between the Earth and the Sun, this would refer to an elongation of 0 degrees (also the primary position of the moon during a solar eclipse). Consequently, its opposite position on the other side of the Earth would be 180 degrees (lunar eclipse for the moon).

Figure 39 shows the Fourier transform of 2002 HK12's lightcurve. The best fit period is 12.73 +/-0.006 hours for the rotational period of 2002 HK12. This was achieved after an 8th order Fourier fit to the asteroid's composite lightcurve. An 8th order fit was possible because this object had many nights' worth of tracking and observation.

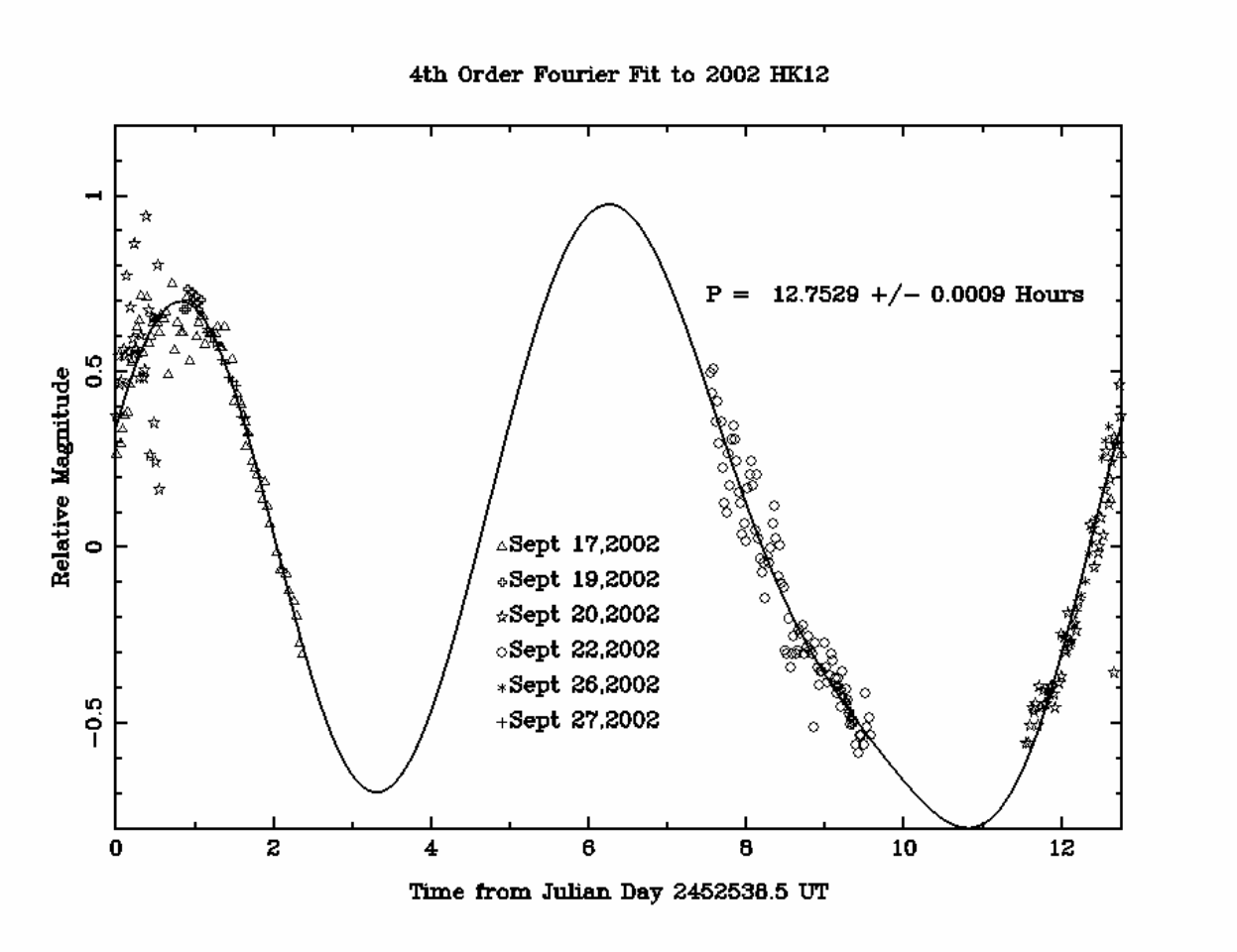

Figure 39. Composite Lightcurve for 2002 HK12

The amplitude of 2002 HK12's lightcurve was 1.6 mag, the largest of the sample. The axial ratio of *a:b* for two of the axes of the asteroid was determined to be 4.4. This elongated

shape (much like an egg or football) is consistent with the large period (12.73 hours) and the large lightcurve amplitude (1.6 mag).

The color measurements of 2002 HK12 are indicative of an S-type. The B-V of 1.12 indicates a red, silicon and iron-rich object. Its J-H of 0.25 indicates that there was minimal thermal emission from the object, which would be much stronger with C-types. As an Apollo asteroid, its orbit is well away from the Main-Belt asteroids, where carbon is more plentiful. Its albedo of 0.08, while relatively moderate, still falls within the range of possible S-type asteroids (Magnusson et al. 1988).

The BVR broadband spectrum of 2002 HK12 had a principal component slope of 0.22mag/100nm. This was the slope of the initial straight-line segment of the spectra in Figure 38. S-types are known to have slopes of 0.3-0.6 mag/100nm. 2002 HK12 is therefore indicative of an S-type. The peak at around 700 nm is also very characteristic of S-types in the NEA population (Bus et al. 2002). Because all of the methods used in this project suggest that 2002 HK12 is an S-type, it is concluded with high confidence that 2002 HK12 is an S-type Near-Earth Object. Confidence levels were assigned based upon the color index, albedo, and broadband slope. If all three data supported a certain taxonomic class, then that NEO was assigned with a high confidence level. If only two data supported a certain type, then the NEO was classified with moderate confidence. Confidence levels were fair for those objects that did not have any infrared data, and consequently no albedo measurements.

2002 HK12's chemical composition must be high in iron, silicon, or both. A common form of silicon in the S-type is the chemical pyroxene, which is seen in a majority of NEAs.

2000 BF19 2000 BF19 is an Apollo asteroid that was classified as a "Potentially Hazardous Asteroid" (PHA) when it was first discovered in 2000. Since then, its orbit (which is continually changing by small amounts) has been re-calculated and is currently no longer considered hazardous. Its movement during this observing run was directed in a westerly direction at approximately 2.2"/min.

The composite lightcurve of 2000 BF19 in Figure 40 has been fit with a 3rd order Fourier fit. Its period of rotation is 7.814 +/- 0.009 hours. This lightcurve is double peaked, similar to the lightcurve for 2002HK12.

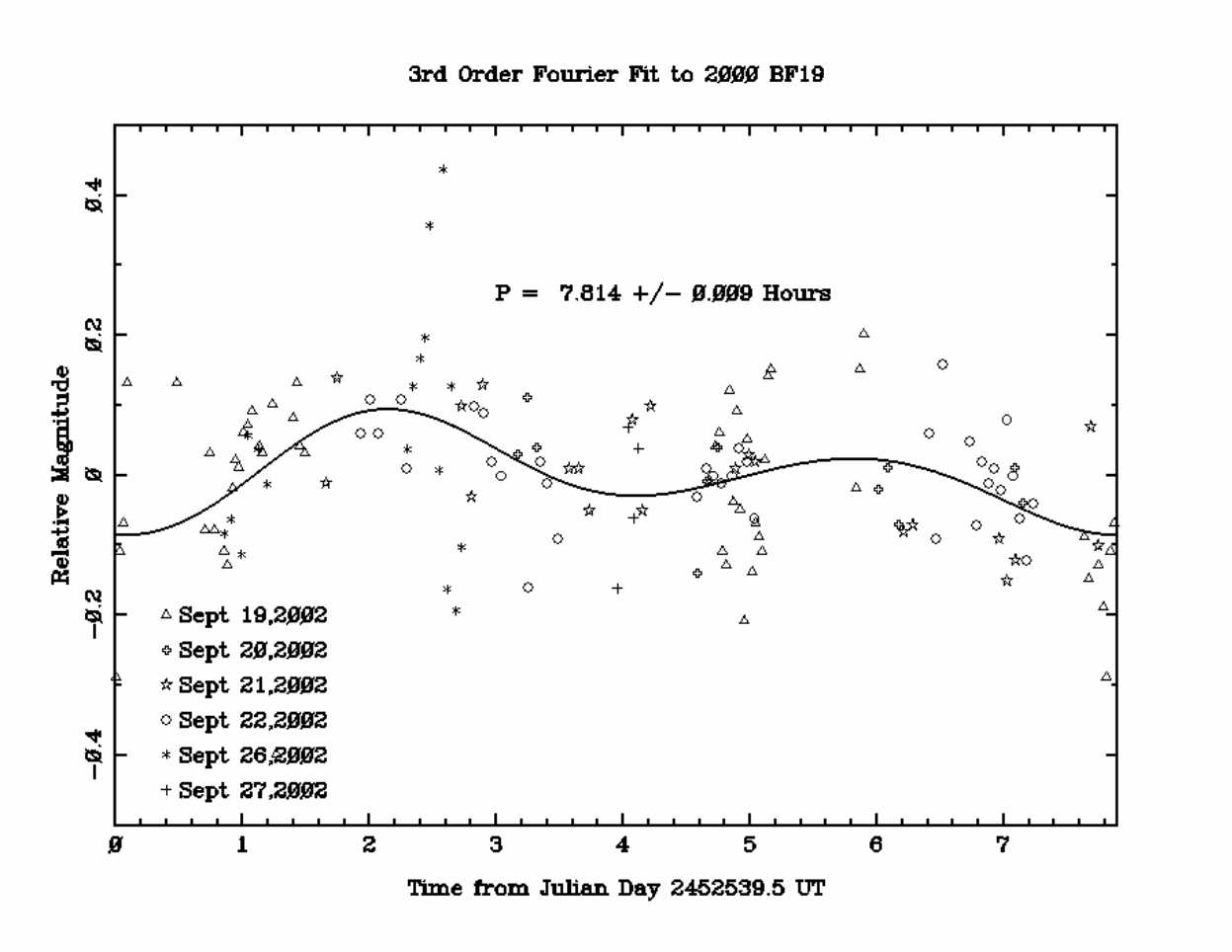

Figure 40. Composite Lightcurve for 2000 BF19

The lightcurve amplitude of 2000 BF19 is 0.18 mag, significantly less than that of 2002 HK12. The corresponding axial ratio of this object is 1.2, making this object nearly spherical. This spherical shape suggests that it has not undergone many significant collisions during its lifetime, causing it to remain spherical and intact (Cunningham 1988). Such an asteroid is significant because it has not changed since the formation of the Solar System. While 2002 HK12's interior is probably exposed due to collisions, 2000 BF19 might offer insight into the primitive nature of asteroids billions of years ago.

Most spherical objects are primitive, C-type, and come from the outer regions of the Main Belt. 2000 BF19, however, is an Apollo, and has a very red surface with high albedo of 0.12. Based on the findings here, it is possible to surmise that 2000 BF19 reflects a significant amount of incident radiation from the Sun without heating and re-radiating in the infrared. Its orbit stays close to Earth.

2000 BF19 is the reddest member of the sample with a B-V=1.23. Its J-H color of 0.18 was smaller than the J-H of 2002 HK12; consequently, it emitted less infrared radiation. Because of its red features, 2000 BF19 must have high concentrations of iron on its surface.

The spectral slope also suggests the presence of iron or silicon minerals on the surface of 2000 BF19. Its value of 0.28 mag/100nm, similar to 2002 HK12's, is indicative of an S-type. The sharp upward slope in the principal component and the sharp downward slope afterwards (Figure 37) is similar to an A-type, a rare type whose reflectance peaks at a waveband centered at 700 nm but falls off after rapidly this waveband. This type of asteroid is a very metallic version of an S-type. There are actually S-types that exhibit similar properties, and so a "hybrid" system was developed after Tholen established the original classes in 1984. S-types could be "Sa,"

which implies an S-type with properties similar to an A-type. This project endeavors to *constrain* a rough taxonomic classification of the NEO; consequently, 2000 BF19 is classified as an S-type in this paper.

2000 BF19's steep slope, red color indices and high albedo lead to its classification as an S-type with high confidence.

2002 KH3 Discovered on May 22, 2002, by the Lincoln Near-Earth Asteroid Research Program (LINEAR) of MIT, 2002 KH3 is an Amor asteroid that was observed in September 2002 with a solar elongation angle of 150 degrees. Its orbit never actually reaches Earth's. Its proper motion of less than an arcmin/second was slower than either 2002 HK12 or 2000 BF19, which made it easier to track. This slower movement can also imply a longer period of rotation (Binzel et al. 1989). However, the period calculated was unexpectedly the shortest of the sample. From a fourth order fit of the Fourier analysis, the period was determined to be 2.773 +/- 0.013 hours (see Figure 41).

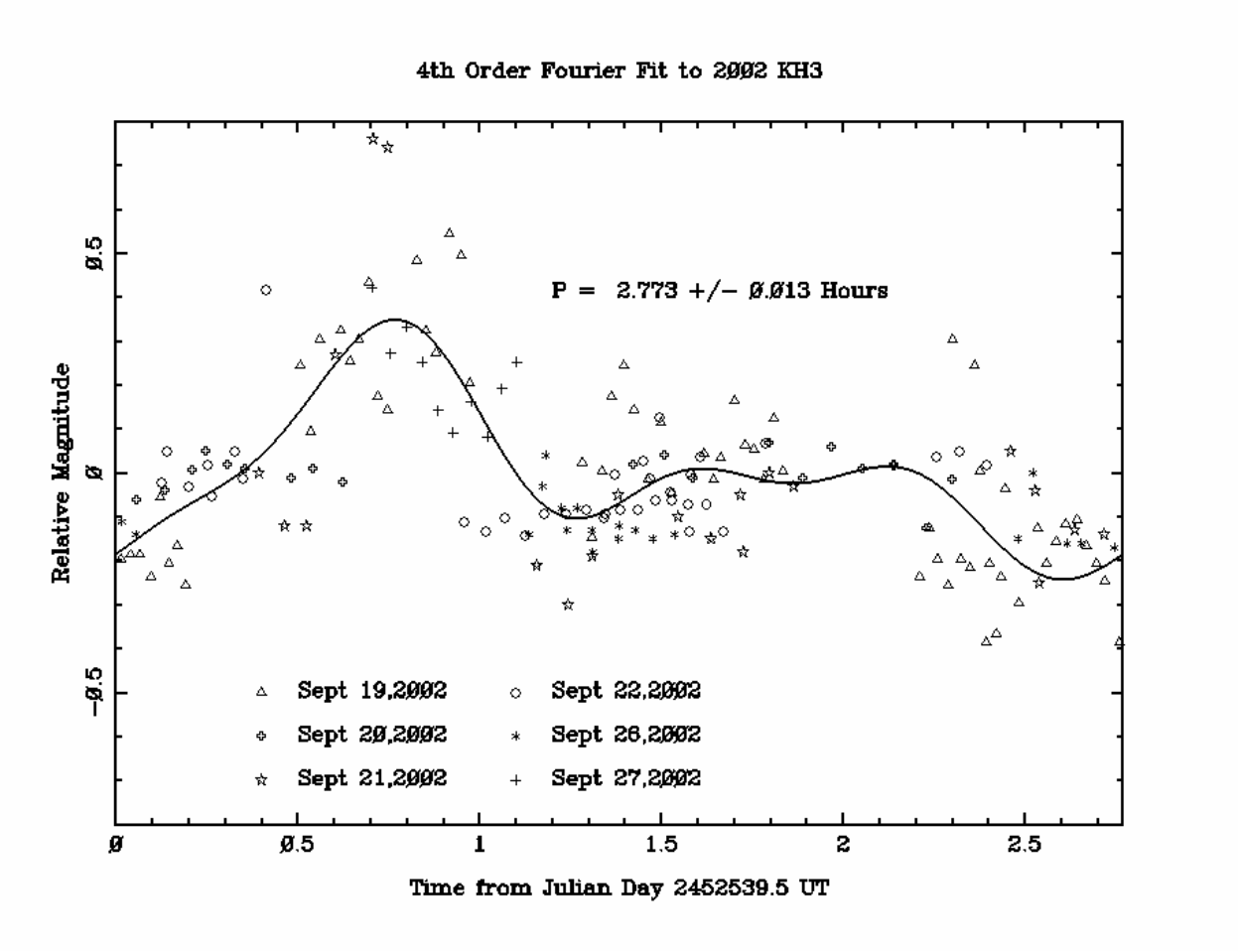

Figure 41. Composite Lightcurve for 2002 KH3

Its lightcurve amplitude was 0.7 mag, and had an axial ratio of 1.9. From this axial ratio, it is a fairly ellipsoidal object, though not nearly as much as 2002 HK12. Its composite lightcurve period was triple-peaked, similar to the triple peak of 2002 HK12.

The albedo of 2002 KH3 was the lowest of the past three members. Its B-V color index was about as red as 2000 BF19 and 2002 HK12. It possibly re-radiates more heat than the other two, due to its lower albedo and larger J-H index of 0.36.

Similarly to 2002 HK12 or 2000 BF19, the spectral slope of 2002 KH3 was also indicative of an S-type. The slope's numerical value is 0.20mag/100nm, only slightly less than

2002 HK12 or 2000 BF19. The red B-V color index and steep slope are indicative of an S-type. Because its albedo was mid-way in the range of possible S-type or C-type asteroids, it is classified as an S-type with only moderate confidence.

2002 PY39 This Amor orbiter was discovered by the JPL/NEAT Team on August 8, 2002, only a month before the observing run was completed in Arizona. 2002 PY39 was not studied with the KPNO infrared telescope due to limited time allotted. Consequently, there are no albedo measurements, but its B-V color index of 1.04 indicates that it is also very red. The BVR spectrum (Figure 38) shows that it has a steep slope of 0.27 mag/100nm, similar to 2000 BF19. From the composite first Fourier fit, it has a period of 7.130+/-0.016 hours (Figure 42). A first-order fit was the best possible fit because only two nights' worth of data were gathered on this object.

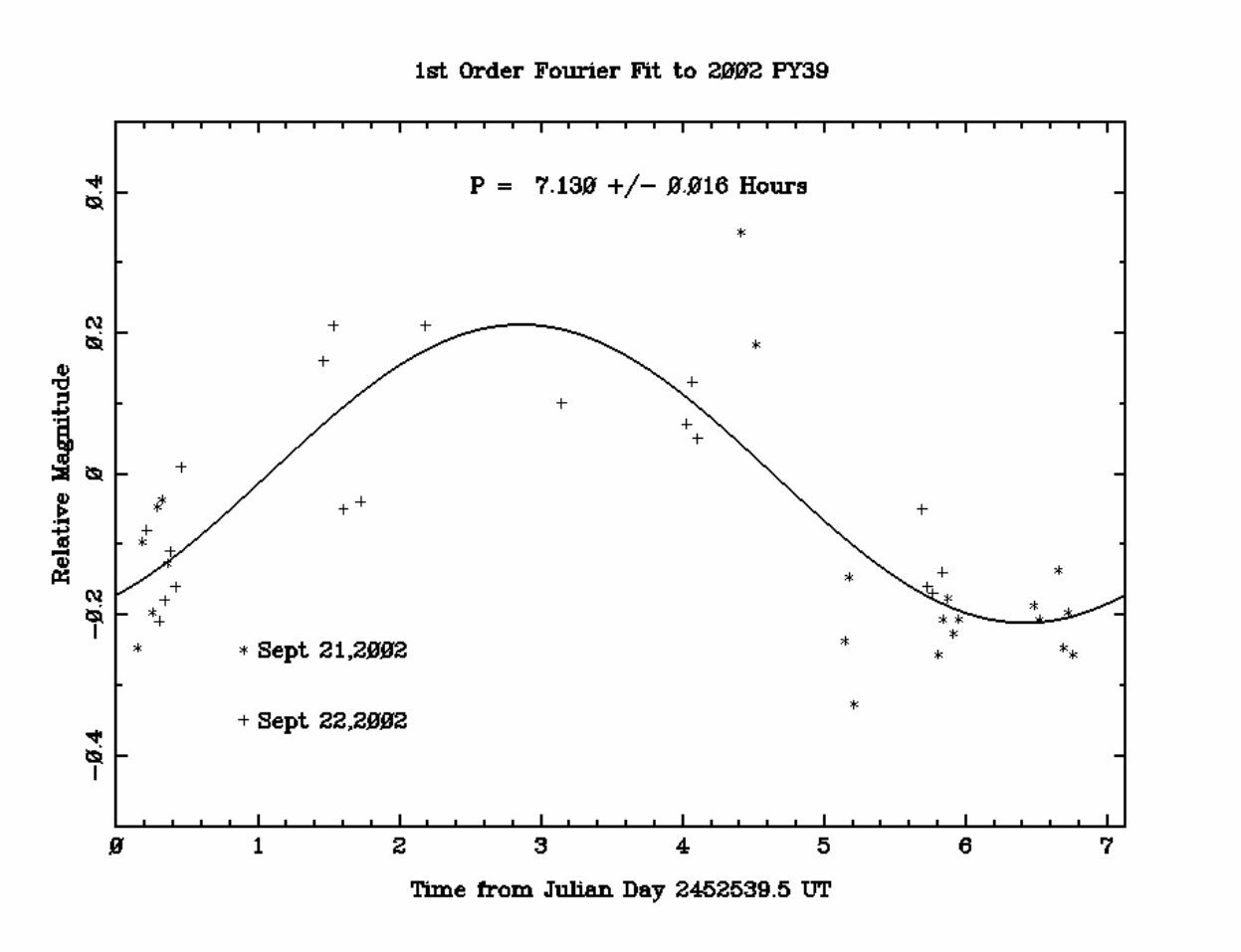

Figure 42. Composite Lightcurve for 2002 PY39

The relatively low lightcurve amplitude of 0.4 mag implies an axial ratio of 1.4, making it only slightly ellipsoidal. Very red B-V color index and steep spectral slope place this object in the S-type bin, but only with fair confidence, since no albedo measurements exist for it.

2002 KH4 This Amor may have had an interesting lightcurve, but it was lost by the Super-LOTIS telescope. It was discovered on May 22, 2002 by LINEAR. Unfortunately, the only data gathered on it was its optical color indices. However, this object's B-V index of 0.41 makes it a

strong candidate for a C-type. Its corresponding spectral slope of -0.14, much different from the other objects in the sample, was characteristic of C-type asteroids.

Table 21 lists a summary of all results for the members of this sample.

Asteroid	Period (hr)	Axial Ratio	B-V (upper limit)	J-H/H-K color indices	Albedo (lower limit)	Slope (upper limit)
2002 HK12	12.73	4.37	1.17	0.25/0.12	0.083	22
2000 BF19	7.81	1.18	1.23	0.18/0.23	0.12	28
2002 KH3	2.77	1.91	1.28	0.36/0.032	0.07	2
2002 PY39	7.13	1.44	0.99	N/A	N/A	N/A
2002 KH4	N/A	N/A	0.41	N/A	N/A	N/A

Table 21. Summary of results for NEO sample

10. CONCLUSIONS

Asteroid	Class Assigned	Confidence Level
2002 HK12	S	High
2000 BF19	S	High
2002 KH3	S	Moderate
2002 PY39	S	Fair
2002 KH4	C	Fair

Table 22. Taxonomic classifications of NEO sample

Table 22 summarizes the taxonomic classifications made in this project. From the analysis, two NEOs were classified as S-types with high confidence, one member classified as S-type with moderate confidence, one member classified as an S-type with fair confidence, and one member classified as a possible C-type. 2002 KH4 needs further observations to better constrain its classification, and thus remains for future investigation.

The relatively short period of 2002 KH3 and elongated shape of 2002 HK12 are intriguing and deserve further study. It is odd that 2002 KH3 has such a relatively short period

since the majority of S-types have longer periods. Its slow proper motion would also suggest that it has a slower rotation rate. 2002 HK12's own physical shape is unique. During its lifetime it must have been a part of a dense asteroid field where multiple collisions caused it to have such an elongated shape.

Equally as interesting is the spherical shape of 2000 BF19. Most S-types have somewhat distorted shapes, but this one has a shape that is nearly spherical. It would be interesting to pin down how it arrived to the NEO population and how it encountered so few (if any) collisions in arriving to the inner Solar System.

The results here do confirm the theory that the majority of Near-Earth Objects are S-types, while the majority of C-types reside in the outer Main Belt of the Solar System.

Work in analysis of NEOs should and must be intensified in order for a broader understanding to come from these physical property studies. Hundreds of Near-Earth Asteroids are known to date, with only a few that have any physical properties recorded. With the wealth of information they can offer and the resources that they can provide, it would be futile to leave this field of science untapped. Although work in this field of science is growing each year, the number of NEOs being discovered is also just as great.

Now that a "first time" trip has been made to Kitt Peak, a second trip would be very beneficial for continuing research that has only just begun. These objects could be investigated further with the larger 4-meter infrared telescope at KPNO. By applying for time at this telescope, it will be possible to make mid-infrared measurements, and get much more accurate albedo measurements for the sample. Such data may help to classify 2002 KH4. This could be important since it may be one of the elusive C-types.

The more NEOs are studied, the better humanity will understand the Solar System in which they live. Studying these numerous and mysterious objects may lead to a better understanding of how humanity's future will unravel. In the words of the NSF Director Dr. Joseph Bordogna, "The future is never easy to 'see.' Nevertheless, the chances of having good vision are much better if you understand the larger context in which you work... Learning to read the larger context gives you a path for imagining the future." [24]

[24] NSF Deputy Director Joseph Bordogna at ABET Annual Meeting, October 1999

11. BIBLIOGRAPHY

Alfven, H. 1964, Icarus, 3, 52

Alvarez, L.W., Alvarez, W.A., F., M., H.V. 1980, Science, 208, 1095.

Angeli, C.A., Guimaraes, T.A., Lazzaro, D. 2001, AJ, 121, 2245-2252.

Barucci, M.A., Lazzarin, M., Tozzi, G.P. 1999, AJ, 117, 1929-1932.

Bell, J.F., Hawke, B.R., Gradie, J.C., McCord, J.B. and Gaffey, M.J. 1985, PASP, 97, 892.

Binzel, R.P. 1989, "Overview of the Asteroids," in *Asteroids II*, ed. R.P. Binzel, T. Gehrels, M.S. Matthews, (Tucson: Univeristy of Arizona Press), 3-18

Binzel, R.P., Harris, A.W., Bus, S.J., Burbine, T.H. 2001, Icarus, 151, 139-149

Binzel, R., Lupishko, D.F., DiMartino, M., Whiteley, R.J., Hahn, G.J. 2002, "Physical Properties of Near-Earth Objects," in *Asteroids III*, ed. W.F. Bottke, A. Cellino, P. Paolicchi, R.P. Binzel, (Tucson: University of Arizona Press), 255-271

Baschek, B. and A. Unsold. *The Near Cosmos, 4th Edition*. New York: Springer-Verlag, 1991.

Britt, D.T. 2000, in Near-Earth Asteroid Sample Return Workshop 1, Surface Processes and Sample Return: What Can We Learn About Asteroid Regoliths? Ed. C.M. Pieters & D.W.G. Sears (Houston: NEASRW), 8007

Burns, J.A. and Tedesco, E.F. 1979, *Asteroids*. (Tucson: University of Arizona Press), 494.11

Bus, S.J., Vilas, F., Barucci, M.A. 2002, "Visible-Wavelength Spectroscopy of Asteroids," in *Asteroids III*, ed. W.F. Bottke, A. Cellino, P. Paolicchi, R.P. Binzel, (Tucson: University of Arizona Press), 255-271

Campbell, D., 2000. Trident Project Thesis, 272, U.S. Naval Academy

Chyba, C.F. 1990, Nature, 343, 129

Cunningham, C.J. ,1988, *Introduction to Asteroids*. Richmond: Willmann-Bell, Inc

Dahlgren, M., Lagerkvist, C.I., Fitzsimmons, A., Williams, I.P., Gordon, M. 1997 A&A, 323, 609-619

Davis, L.E. *A User's Guide to the IRAF Apphot Package*. National Optical Astronomical Observatories, 1989.

Davis, L.E., Massey, P. *A User's Guide to Stellar CCD Photometry with IRAF*. National Optical Astronomical Observatories, 1992.

Dermott, S. and Murray, C. 1982, Nature, 296, 418

DiMartino, M., Carusi, A., Dotto, E., Lazzarin, M., Marzari, F., Migliorini, F. 1997, A&A, 329, 1145-1151

Dunham, D.W., Binzel, R.P. 1990, ApJ, 99, 5

D'urech 2000, Icarus, Volume 159, Issue 1, p. 192-196.

Fernandez, Y.R., Jewitt, D.C., Sheppard, S.S. 2001, ApJ, 553, L197-L200

Franchi, I.A., Baker, I., Wright, I.P., Pillinger, C.T. 2000, in Near-Earth Asteroid Sample Return Workshop, High Precision Light Element Characterization of Asteroidal Material, ed. C.M. Pieters & D.W.G. Sears (Houston: NEASRW), 8018

Gaffey, M.J., Bell, J.F., Cruikshank, D.P. 1989 "Reflectance Spectroscopy and Asteroid Surface Mineralogy," in *Asteroids II*, 1989, ed. R.P. Binzel, T. Gehrels, M.S. Matthews, (Tucson: University of Arizona Press)

Grieve, R.A.F. & Shoemaker, E.M. 1994, in *Hazards Due to Comets and Asteroids*, ed. T. Gehrels (Tuscon: University of Arizona), 417

Harris, A.W. 1985, ACM II, Uppsala

Harris, A.W., Delbo, M., Binzel, R.P., Davies, J.K., Roberts, J., Tholen, D.J., Whitely, R.J., 2001, Icarus, 153, 332-337

Harris, A.W., Lupishko, D.F. 1989 "Photometric Lightcurve Observations and Reduction Technique," in *Asteroids II*, ed. R.P. Binzel, T. Gehrels, M.S. Matthews, (Tucson: University of Arizona Press)

Hicks, M.D., Buratti, B.J., Newburn, R.L., Rabinowitz, D.L. 2000, Icarus, 143, 354-359

Hicks, M.D., Buratti, B.J., Rabinowitz, D.L., Weissman, P.R., Doressoudiram, A., Fink, U., 1999, in Lunar and Planetary Science Conference 30, The Deep Space 1 Mission Target 1992 KD: A Connection to Stony Meteorites? Ed. C.B. Agee & D.C. Black (Houston: LPI), 1719

Hills, J.G. & Goda, M.P. 1993, AJ, 105, 1114

Hiltner, J. *Astronomical Techniques.* Chicago: University of Chicago Press, 1964.

Hunten, D.M., 1993, Science, 259, 915

Kartunnen, H., Kroger, P., Oja, H., and M. Poutanen. *Fundamental Astronomy*. New York: New York: Springer-Verlag, 1987.

Kowal, C. T. 1988, *Asteroids: Their Nature and Utilization*, (New York: Halsted Press)

Lagerkvist, C.I. 1983, ACM, 11

Lazzarin, M., Barbieri, Barucci, M.A., 1995, AJ, 110, 6

Lazzarin, M., DiMartino, M., Barucci, M.A., Doressoundiram, A., Florczak 2001, A&A, 327, 388-391

Leake, M., Gradie, J., Morrison, D. 1978, Meteoritics, 13, 101-119

Lupishko, D.F. 2000, in Catastrophic Events Conference, Physical Properties of Near-Earth Asteroids as Principal Impactors onto the Earth, ed. F. Brandstatter, H. Haber & C. Koeberl (Vienna, Austria: CEC), 3040

Lupishko, D.F., Lupishko, T.A., 2001, in Catastrophic Events Conference, Asteroid Hazard: Core of the Problem, ed. F. Brandstatter, H. Haber & C. Koeberl (Vienna, Austria: CEC), 3039

Magnusson, P., Barucci, M.A., Drummond, J.D., Lumme, K., Ostro, S.J., Surdej, J., Taylor, R.C., Zappala, V. 1988, "Determination of Pole Orientations and Shapes of Asteroids," in *Asteroids II*, ed. Ed. W.F. Bottke, A. Cellino, P. Paolicchi, R.P. Binzel, (Tucson: University of Arizona Press), 255-271

Marcus, J.N. & Olsen, M.A., 1991, in *Comets in the Post-Halley Era*, vol. 1, eds. R.L. Newburn, Jr., M. Neugebauer, & J. Rahe (Dordrecht: Kluwer)

Michalowski, T. 1993, Icarus, 106, 563-572

Moore, Patrick. *Astronomy & Space: Volume 1*. New York: Neale Watson Academic Publications, Inc.

Morrison, D. ed. 1992, The Spaceguard Survey: Report of the NASA International Near-Earth Object Detection Workshop (Pasadena: Jet Propulsion Laboratory)

Morbidelli, A., Jedicke, R., Bottke, W.F., Michel, P., Tedesco, E.F. 2002, Icarus, 158, 329-342

Ostro, S.J. 1986, Lunar & Planetary Institute, 17, 636-637

Rabinowitz, D.L., 1998, Icarus, 134, 342-346

Richmond, Michael. Online Physics Notes

Rietmeijer, F.J., Nuth, J.A. 2000, in Near-Earth Asteroid Sample Return Workshop, The Scientific Case for Sample Return From a Primitive Near-Earth Asteroid, ed.

C.M. Pieters & D.W.G. Sears (Houston: NEASRW), 8005

Shoemaker, E., Canavan, G., Darrah, J., Harris, A., Morrison, D., Mumma, M., & Rabinowitz, D. 1995, in Report of Near-Earth Object Survey Working Group 1, ed. D. Morrison (California: NASA)

Tedesco, E.F., and Zappala, V. 1980, Icarus, 43, 33

Tholen, D.J. 1984, PhD thesis, University of Arizona

Veeder, G.J., Matson, D.L., Hoover, G. 1983, AJ, 88, 1060-1063

Vilas, F., Larsen, S.M., Hatch, E.C. Jarvis, K.S. 1993, Icarus, 105, 67-78

Weissman, P.R. O'Hearn, McFadden, Rickman 1989, "Evolution of Comets into Asteroids," in *Asteroids II*, ed. R.P. Binzel, T. Gehrels, M.S. Matthews, (Tucson: University of Arizona Press)

Wetherill, G.W., Chambers, J.E., 1999, in 63rd Annual Meteoritical Society Meeting, Formation of the Asteroids, ed. A.M. Davis & M. Wadhwa (Chicago: AMS), 5227

Whiteley, R. J. 2001, Ph.D. thesis, Univ. Hawaii

Whiteley, R.J., Tholen, D.J., Hergenrother, C.W.: Icarus, Volume 157, Issue 1, pp. 139-154 (2002)

Wisniewski, W.Z., Michalowski, T.M., Harris, A.W., McMillan, R.S., 1996, Icarus, 126, 395-449

Zeilik, M., Gregory, S. 1998, *Introductory Astronomy and Astrophysics*, (Philadelphia: Saunders College Publishing)

12. APPENDIX

Figures 43-45 show the confidence in the assignment of the period to each member of the sample, based upon the Fourier fit from the lightcurve data. The "strength parameter" is an indicator of which period from the fit was the most probable period of the object. The period corresponding to a strength parameter closest to one was chosen as the published period in this paper. A strength parameter of one corresponded to a fit that was within one sigma standard deviation from the data points. Figure 43 shows such a fitting process on the fourth order fitting for 2002 HK12.

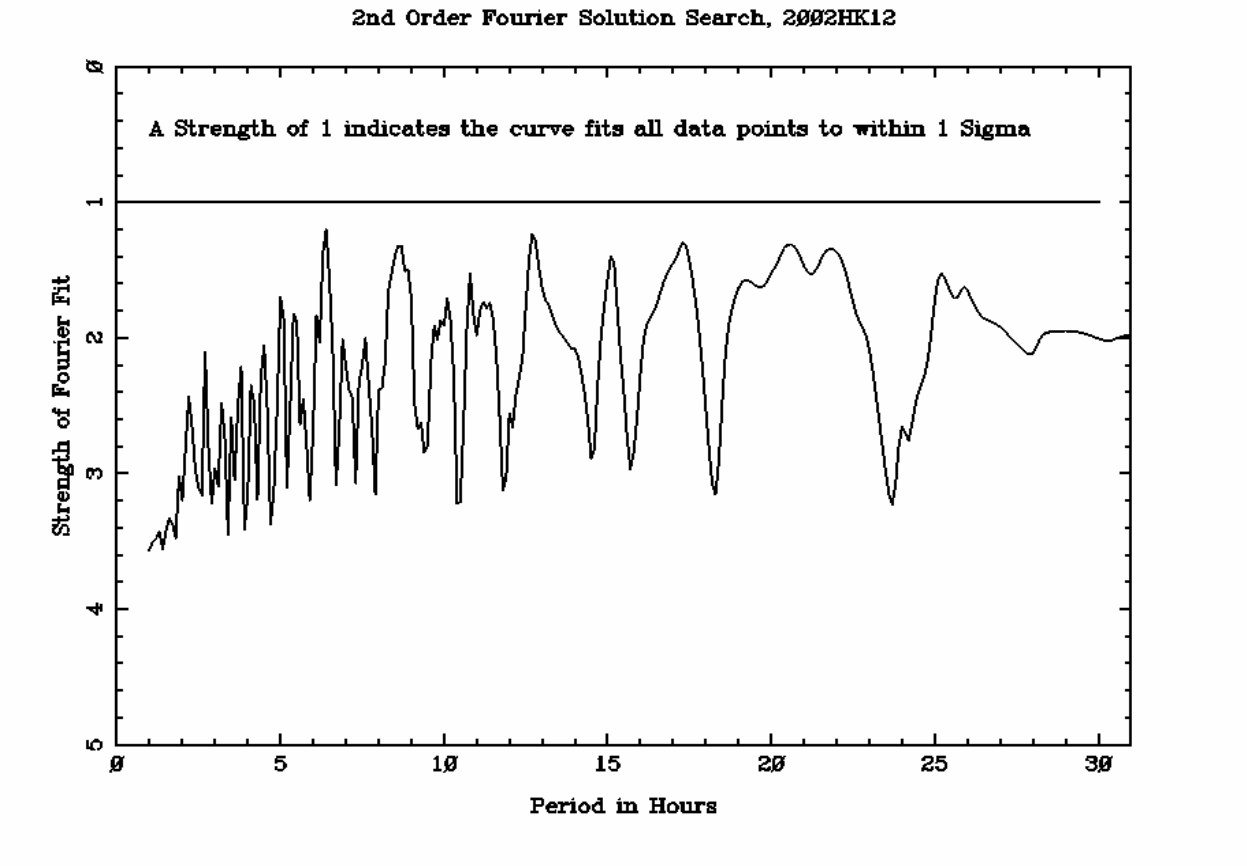

Figure 43. Fourth-order strength parameter for 2002 HK12

Similar strength parameters are shown for 2000 BF19 and 2003 PY39 (Figures 44-45). Both 2002 HK12 and 2000 BF19 had many possible periods with similar strength parameters, close to a value of 1.

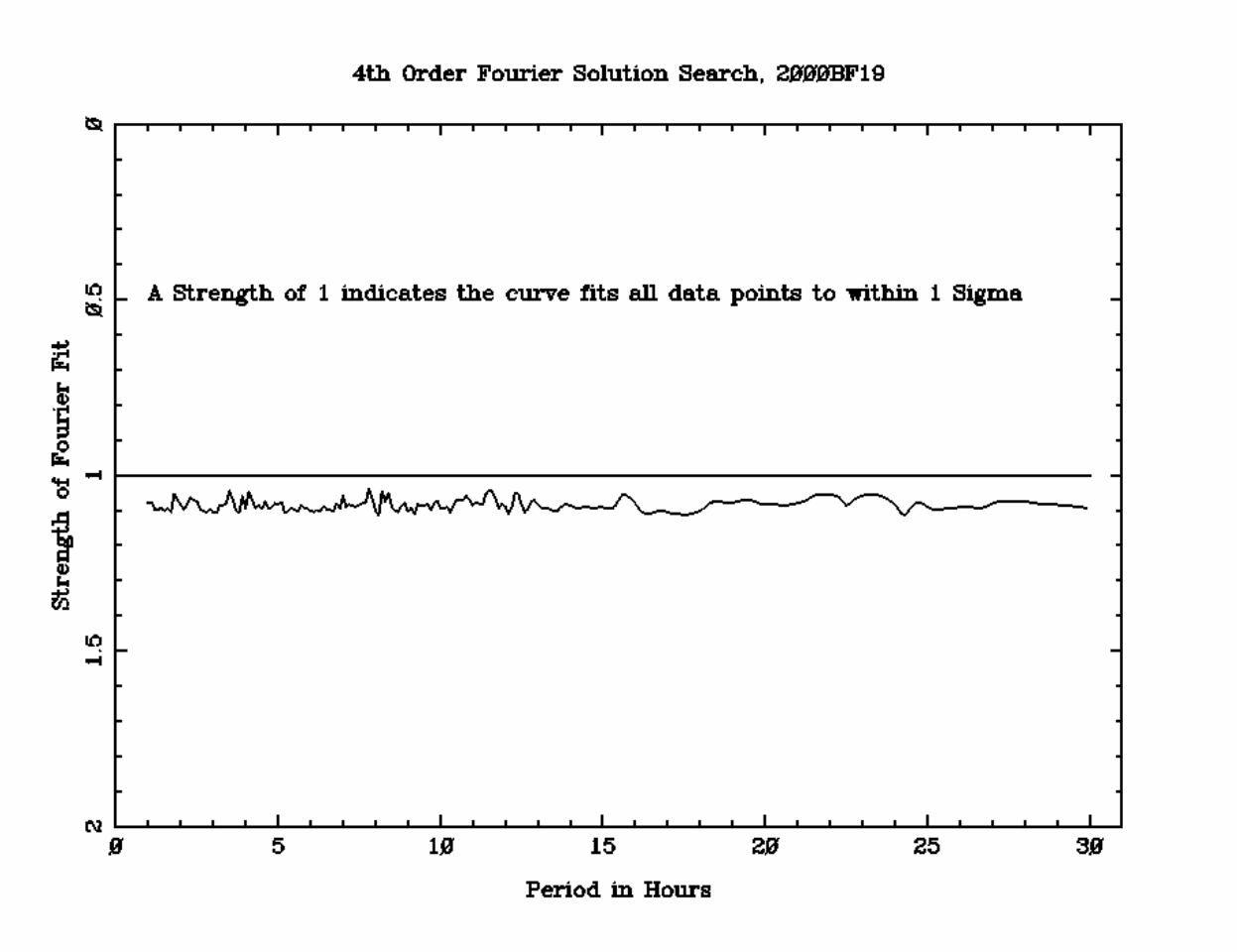

Figure 44. Fourth-order strength parameter for 2000 BF19

2002 PY39's strength parameter (Figure 45) was much more obvious as to which period was the most probable.

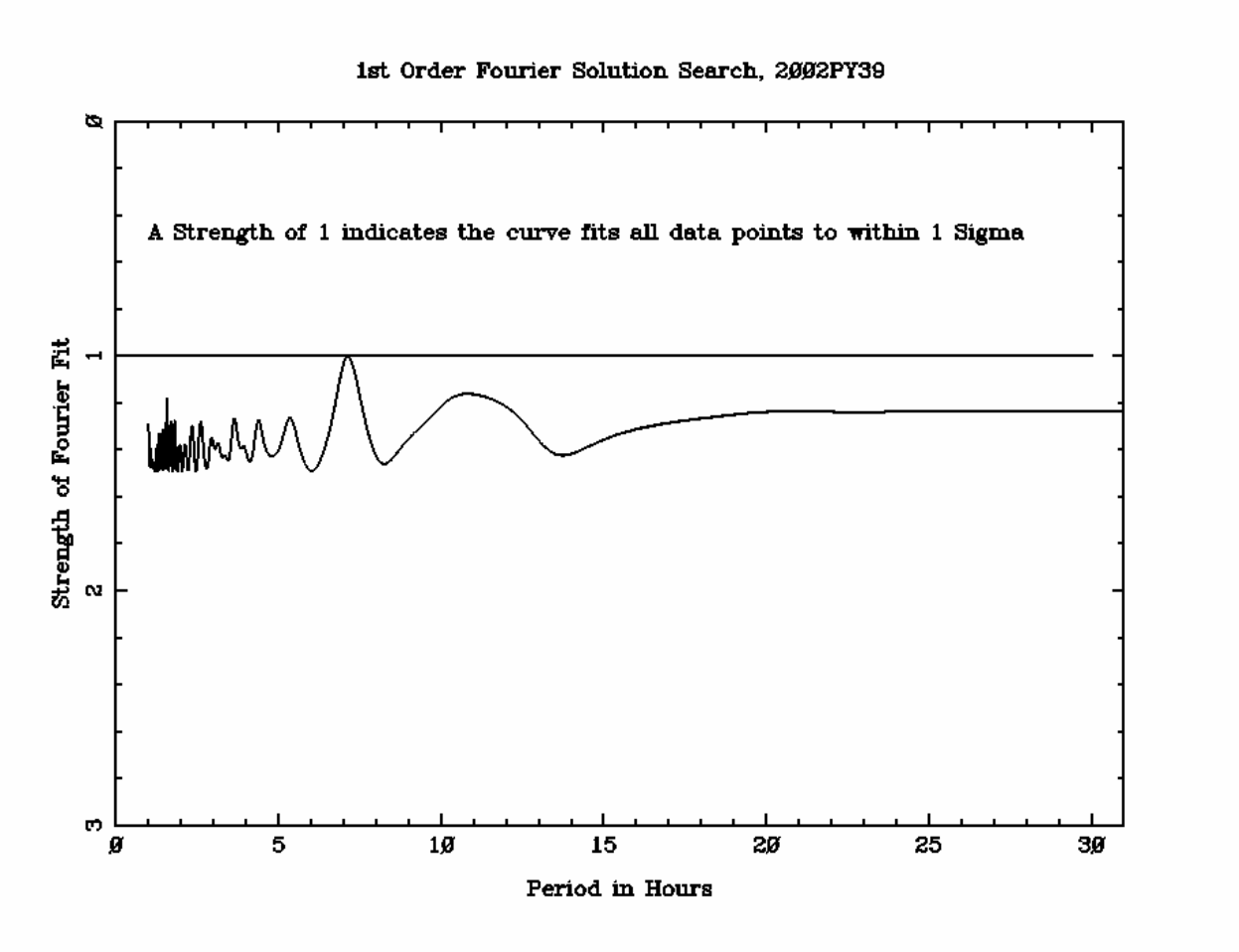

Figure 45. First order strength parameter for 2002 PY39

The following data were used to construct the composite lightcurves of the NEO sample (excluding 2002 KH4). The left side of each column is time in hours (starting from t=0), and the right side of each column is magnitude, relative to the first image of the set of data.

2002 HK12

Time(hr)	Relative Magnitude
0.0000	0.6773
0.0318	0.7194
0.0636	0.7588
0.0954	0.7945
0.1272	0.8258
0.1590	0.8519
0.1908	0.8725
0.2226	0.8873
0.2544	0.8963
0.2862	0.8998
0.3180	0.8981
0.3498	0.8919
0.3817	0.8821
0.4135	0.8695
0.4453	0.8551
0.4771	0.8401
0.5089	0.8254
0.5407	0.8119
0.5725	0.8003
0.6043	0.7915
0.6361	0.7856
0.6679	0.7829
0.6997	0.7833
0.7315	0.7866
0.7633	0.7921
0.7951	0.7993
0.8269	0.8073
0.8587	0.8152
0.8905	0.8219
0.9223	0.8266
0.9541	0.8283
0.9859	0.8263
1.0177	0.8198
1.0495	0.8086
1.0814	0.7923
1.1132	0.7710
1.1450	0.7448
1.1768	0.7143
1.2086	0.6801
1.2404	0.6429
1.2722	0.6037
1.3040	0.5632
1.3358	0.5226
1.3676	0.4827
1.3994	0.4443
1.4312	0.4082
1.4630	0.3748
1.4948	0.3445
1.5266	0.3175
1.5584	0.2937
1.5902	0.2730
1.6220	0.2548
1.6538	0.2388
1.6856	0.2244
1.7174	0.2108
1.7492	0.1975
1.7811	0.1838
1.8129	0.1691
1.8447	0.1529
1.8765	0.1351
1.9083	0.1153
1.9401	0.0936
1.9719	0.0700
2.0037	0.0449
2.0355	0.0187
2.0673	-0.0082
2.0991	-0.0353
2.1309	-0.0619
2.1627	-0.0875
2.1945	-0.1117
2.2263	-0.1339
2.2581	-0.1538
2.2899	-0.1712
2.3217	-0.1861
2.3535	-0.1984
2.3853	-0.2084
2.4171	-0.2163
2.4489	-0.2225
2.4808	-0.2275
2.5126	-0.2318
2.5444	-0.2358
2.5762	-0.2400
2.6080	-0.2448
2.6398	-0.2506
2.6716	-0.2575
2.7034	-0.2659
2.7352	-0.2756
2.7670	-0.2866
2.7988	-0.2988
2.8306	-0.3119
2.8624	-0.3256
2.8942	-0.3396
2.9260	-0.3535
2.9578	-0.3670
2.9896	-0.3799
3.0214	-0.3919
3.0532	-0.4028
3.0850	-0.4127
3.1168	-0.4215
3.1486	-0.4293
3.1805	-0.4364
3.2123	-0.4430
3.2441	-0.4493
3.2759	-0.4558
3.3077	-0.4627
3.3395	-0.4703
3.3713	-0.4788
3.4031	-0.4885
3.4349	-0.4993
3.4667	-0.5113
3.4985	-0.5244
3.5303	-0.5385
3.5621	-0.5532
3.5939	-0.5683
3.6257	-0.5835
3.6575	-0.5983
3.6893	-0.6124
3.7211	-0.6256
3.7529	-0.6374
3.7847	-0.6478
3.8165	-0.6566
3.8483	-0.6637
3.8802	-0.6693
3.9120	-0.6735
3.9438	-0.6764
3.9756	-0.6783
4.0074	-0.6796
4.0392	-0.6805
4.0710	-0.6813
4.1028	-0.6823
4.1346	-0.6836
4.1664	-0.6853
4.1982	-0.6875
4.2300	-0.6899
4.2618	-0.6925
4.2936	-0.6949
4.3254	-0.6968
4.3572	-0.6976
4.3890	-0.6970
4.4208	-0.6945
4.4526	-0.6895
4.4844	-0.6818
4.5162	-0.6710
4.5480	-0.6570
4.5799	-0.6395
4.6117	-0.6188
4.6435	-0.5950

2002 HK12 (cont'd)

Time(hr)	Relative Magnitude
4.6753	-0.5685
4.7071	-0.5397
4.7389	-0.5092
4.7707	-0.4776
4.8025	-0.4457
4.8343	-0.4140
4.8661	-0.3834
4.8979	-0.3543
4.9297	-0.3274
4.9615	-0.3029
4.9933	-0.2812
5.0251	-0.2624
5.0569	-0.2464
5.0887	-0.2330
5.1205	-0.2219
5.1523	-0.2126
5.1841	-0.2047
5.2159	-0.1975
5.2477	-0.1905
5.2796	-0.1831
5.3114	-0.1747
5.3432	-0.1649
5.3750	-0.1535
5.4068	-0.1401
5.4386	-0.1247
5.4704	-0.1073
5.5022	-0.0881
5.5340	-0.0674
5.5658	-0.0454
5.5976	-0.0226
5.6294	0.0007
5.6612	0.0240
5.6930	0.0470
5.7248	0.0695
5.7566	0.0913
5.7884	0.1123
5.8202	0.1328
5.8520	0.1528
5.8838	0.1726
5.9156	0.1928
5.9474	0.2136
5.9793	0.2358
6.0111	0.2597
6.0429	0.2858
6.0747	0.3145
6.1065	0.3460
6.1383	0.3804
6.1701	0.4177
6.2019	0.4577
6.2337	0.4999
6.2655	0.5437
6.2973	0.5885
6.3291	0.6333
6.3609	0.6773
6.3927	0.7194
6.4245	0.7588
6.4563	0.7945
6.4881	0.8258
6.5199	0.8519
6.5517	0.8725
6.5835	0.8873
6.6153	0.8963
6.6471	0.8998
6.6790	0.8981
6.7108	0.8919
6.7426	0.8821
6.7744	0.8695
6.8062	0.8551
6.8380	0.8401
6.8698	0.8254
6.9016	0.8119
6.9334	0.8003
6.9652	0.7915
6.9970	0.7856

2000 BF19

Time(hr)	Relative Magnitude
0.0000	-0.0854
0.0391	-0.0858
0.0781	-0.0859
0.1172	-0.0858
0.1562	-0.0853
0.1953	-0.0846
0.2343	-0.0837
0.2734	-0.0824
0.3124	-0.0809
0.3515	-0.0790
0.3905	-0.0769
0.4296	-0.0745
0.4686	-0.0719
0.5077	-0.0689
0.5467	-0.0657
0.5858	-0.0623
0.6248	-0.0586
0.6639	-0.0547
0.7029	-0.0506
0.7420	-0.0462
0.7810	-0.0417
0.8201	-0.0370
0.8591	-0.0322
0.8982	-0.0272
0.9372	-0.0221
0.9763	-0.0168
1.0153	-0.0115
1.0544	-0.0062
1.0934	-0.0007
1.1325	0.0047
1.1715	0.0101
1.2106	0.0156
1.2496	0.0210
1.2887	0.0263
1.3277	0.0315
1.3668	0.0367
1.4058	0.0417
1.4449	0.0466
1.4839	0.0513
1.5230	0.0559
1.5620	0.0602
1.6011	0.0644
1.6401	0.0683
1.6792	0.0720
1.7182	0.0754
1.7573	0.0785
1.7963	0.0814
1.8354	0.0840
1.8744	0.0863
1.9135	0.0883
1.9525	0.0900
1.9916	0.0914
2.0306	0.0925
2.0697	0.0932
2.1087	0.0937
2.1478	0.0938
2.1868	0.0936
2.2259	0.0932
2.2649	0.0924
2.3040	0.0913
2.3430	0.0900
2.3821	0.0884
2.4211	0.0865
2.4602	0.0844
2.4992	0.0820
2.5383	0.0794
2.5773	0.0766
2.6164	0.0736
2.6554	0.0705
2.6945	0.0672
2.7335	0.0637
2.7726	0.0601
2.8116	0.0564
2.8507	0.0526
2.8897	0.0488
2.9288	0.0449
2.9678	0.0409
3.0069	0.0369
3.0459	0.0330
3.0850	0.0290
3.1240	0.0251
3.1631	0.0212
3.2021	0.0174
3.2412	0.0137
3.2802	0.0101
3.3193	0.0065
3.3583	0.0031
3.3974	-0.0002
3.4364	-0.0033
3.4755	-0.0063
3.5145	-0.0092
3.5536	-0.0119
3.5926	-0.0144
3.6317	-0.0167
3.6707	-0.0188
3.7098	-0.0208
3.7488	-0.0226
3.7879	-0.0242
3.8269	-0.0255
3.8660	-0.0267
3.9050	-0.0277
3.9441	-0.0286
3.9831	-0.0292
4.0222	-0.0296
4.0612	-0.0299
4.1003	-0.0300
4.1393	-0.0299
4.1784	-0.0296
4.2174	-0.0292
4.2565	-0.0287
4.2955	-0.0280
4.3346	-0.0271
4.3736	-0.0262
4.4127	-0.0251
4.4517	-0.0239
4.4908	-0.0226
4.5298	-0.0212
4.5689	-0.0197
4.6079	-0.0182
4.6470	-0.0165
4.6861	-0.0148
4.7251	-0.0131
4.7642	-0.0113
4.8032	-0.0095
4.8423	-0.0077
4.8813	-0.0059
4.9204	-0.0040
4.9594	-0.0022
4.9985	-0.0004
5.0375	0.0014
5.0766	0.0032
5.1156	0.0049
5.1547	0.0066
5.1937	0.0083
5.2328	0.0099
5.2718	0.0114
5.3109	0.0129
5.3499	0.0143
5.3890	0.0156
5.4280	0.0168
5.4671	0.0179
5.5061	0.0190
5.5452	0.0199
5.5842	0.0207
5.6233	0.0214
5.6623	0.0220
5.7014	0.0225
5.7404	0.0228
5.7795	0.0231
5.8185	0.0232
5.8576	0.0231
5.8966	0.0229
5.9357	0.0226
5.9747	0.0222
6.0138	0.0216
6.0528	0.0208
6.0919	0.0199
6.1309	0.0189
6.1700	0.0177
6.2090	0.0164
6.2481	0.0149
6.2871	0.0133

2000 BF19 (cont'd)

Time(hr)	Relative Magnitude
6.3262	0.0115
6.3652	0.0097
6.4043	0.0076
6.4433	0.0055
6.4824	0.0032
6.5214	0.0008
6.5605	-0.0017
6.5995	-0.0044
6.6386	-0.0071
6.6776	-0.0100
6.7167	-0.0129
6.7557	-0.0159
6.7948	-0.0190
6.8338	-0.0221
6.8729	-0.0253
6.9119	-0.0286
6.9510	-0.0319
6.9900	-0.0352
7.0291	-0.0385
7.0681	-0.0418
7.1072	-0.0450
7.1462	-0.0483
7.1853	-0.0515
7.2243	-0.0546
7.2634	-0.0577
7.3024	-0.0607
7.3415	-0.0636
7.3805	-0.0663
7.4196	-0.0690
7.4586	-0.0715
7.4977	-0.0738
7.5367	-0.0760
7.5758	-0.0780
7.6148	-0.0798
7.6539	-0.0813
7.6929	-0.0827
7.7320	-0.0838
7.7710	-0.0847
7.8101	-0.0854
7.8491	-0.0858
7.8882	-0.0859
7.9272	-0.0858
7.9663	-0.0853
8.0054	-0.0846
8.0444	-0.0837
8.0835	-0.0824
8.1225	-0.0809
8.1616	-0.0790
8.2006	-0.0769
8.2397	-0.0745
8.2787	-0.0719
8.3178	-0.0689
8.3568	-0.0657
8.3959	-0.0623
8.4349	-0.0586
8.4740	-0.0547
8.5130	-0.0506
8.5521	-0.0462
8.5911	-0.0417

2002 KH3

Time(hr)	Relative Magnitude
0.0000	-0.1853
0.0138	-0.1771
0.0277	-0.1687
0.0415	-0.1603
0.0554	-0.1519
0.0693	-0.1435
0.0831	-0.1353
0.0970	-0.1272
0.1108	-0.1192
0.1247	-0.1114
0.1385	-0.1039
0.1524	-0.0966
0.1662	-0.0894
0.1801	-0.0825
0.1939	-0.0757
0.2078	-0.0691
0.2216	-0.0625
0.2355	-0.0560
0.2493	-0.0494
0.2632	-0.0428
0.2770	-0.0360
0.2909	-0.0290
0.3047	-0.0217
0.3186	-0.0141
0.3324	-0.0061
0.3463	0.0024
0.3601	0.0114
0.3740	0.0209
0.3878	0.0309
0.4017	0.0416
0.4155	0.0529
0.4294	0.0648
0.4432	0.0773
0.4571	0.0904
0.4709	0.1041
0.4848	0.1182
0.4986	0.1328
0.5125	0.1477
0.5263	0.1629
0.5402	0.1783
0.5540	0.1937
0.5678	0.2091
0.5817	0.2244
0.5955	0.2393
0.6094	0.2538
0.6232	0.2678
0.6371	0.2810
0.6509	0.2934
0.6648	0.3049
0.6786	0.3152
0.6925	0.3243
0.7063	0.3321
0.7202	0.3385
0.7340	0.3434
0.7479	0.3466
0.7617	0.3482
0.7756	0.3481
0.7894	0.3463
0.8033	0.3427
0.8171	0.3373
0.8310	0.3303
0.8448	0.3215
0.8587	0.3111
0.8725	0.2992
0.8864	0.2858
0.9002	0.2711
0.9141	0.2551
0.9279	0.2381
0.9418	0.2200
0.9556	0.2012
0.9695	0.1818
0.9833	0.1619
0.9972	0.1417
1.0110	0.1214
1.0249	0.1012
1.0387	0.0811
1.0526	0.0615
1.0664	0.0425
1.0803	0.0242
1.0941	0.0067
1.1080	-0.0098
1.1218	-0.0252
1.1357	-0.0393
1.1495	-0.0522
1.1634	-0.0637
1.1772	-0.0738
1.1911	-0.0824
1.2049	-0.0896
1.2188	-0.0952
1.2326	-0.0994
1.2465	-0.1022
1.2603	-0.1036
1.2742	-0.1037
1.2880	-0.1026
1.3019	-0.1003
1.3157	-0.0970
1.3296	-0.0928
1.3434	-0.0877
1.3573	-0.0820
1.3711	-0.0757
1.3850	-0.0690
1.3988	-0.0619
1.4127	-0.0548
1.4265	-0.0475
1.4404	-0.0404
1.4542	-0.0334
1.4681	-0.0267
1.4819	-0.0205
1.4958	-0.0146
1.5096	-0.0094
1.5235	-0.0047
1.5373	-0.0006
1.5512	0.0027
1.5650	0.0054
1.5789	0.0074
1.5927	0.0087
1.6066	0.0093
1.6204	0.0093
1.6343	0.0087
1.6481	0.0076
1.6620	0.0060
1.6758	0.0040
1.6897	0.0016
1.7035	-0.0010
1.7174	-0.0037
1.7312	-0.0066
1.7451	-0.0094
1.7589	-0.0122
1.7728	-0.0148
1.7866	-0.0172
1.8005	-0.0193
1.8143	-0.0211
1.8282	-0.0225
1.8420	-0.0234
1.8559	-0.0239
1.8697	-0.0239
1.8836	-0.0235
1.8974	-0.0226
1.9113	-0.0212
1.9251	-0.0194
1.9390	-0.0172
1.9528	-0.0147
1.9667	-0.0119
1.9805	-0.0089
1.9944	-0.0057
2.0082	-0.0025
2.0221	0.0006
2.0359	0.0036
2.0498	0.0065
2.0636	0.0090
2.0775	0.0111
2.0913	0.0128
2.1052	0.0139
2.1190	0.0143
2.1329	0.0141
2.1467	0.0131
2.1606	0.0113
2.1744	0.0086
2.1883	0.0051
2.2021	0.0007
2.2160	-0.0046
2.2298	-0.0108

2002 KH3 (cont'd)

Time(hr)	Relative Magnitude
2.2437	-0.0179
2.2575	-0.0258
2.2714	-0.0345
2.2852	-0.0439
2.2991	-0.0539
2.3129	-0.0645
2.3268	-0.0756
2.3406	-0.0871
2.3545	-0.0989
2.3683	-0.1108
2.3822	-0.1229
2.3960	-0.1348
2.4099	-0.1467
2.4237	-0.1582
2.4376	-0.1694
2.4514	-0.1800
2.4653	-0.1901
2.4791	-0.1995
2.4930	-0.2081
2.5068	-0.2159
2.5207	-0.2228
2.5345	-0.2287
2.5484	-0.2336
2.5622	-0.2375
2.5761	-0.2403
2.5899	-0.2421
2.6038	-0.2428
2.6176	-0.2425
2.6315	-0.2411
2.6453	-0.2388
2.6592	-0.2356
2.6730	-0.2316
2.6869	-0.2267
2.7007	-0.2211
2.7146	-0.2149
2.7284	-0.2081
2.7423	-0.2009
2.7561	-0.1932
2.7700	-0.1853
2.7838	-0.1771
2.7977	-0.1687
2.8115	-0.1603
2.8254	-0.1519
2.8392	-0.1435
2.8531	-0.1353
2.8669	-0.1272
2.8808	-0.1192
2.8946	-0.1114
2.9085	-0.1039
2.9223	-0.0966
2.9362	-0.0894
2.9500	-0.0825
2.9639	-0.0757
2.9777	-0.0691
2.9916	-0.0625
3.0054	-0.0560
3.0193	-0.0494
3.0331	-0.0428
3.0470	-0.0360

2002 PY39

Time(hr)	Relative Magnitude
0.0000	-0.1725
0.0356	-0.1685
0.0712	-0.1644
0.1068	-0.1601
0.1424	-0.1557
0.1780	-0.1511
0.2136	-0.1464
0.2492	-0.1415
0.2848	-0.1365
0.3204	-0.1313
0.3560	-0.1261
0.3916	-0.1207
0.4272	-0.1151
0.4628	-0.1095
0.4984	-0.1037
0.5340	-0.0979
0.5696	-0.0919
0.6052	-0.0859
0.6408	-0.0798
0.6764	-0.0736
0.7120	-0.0673
0.7476	-0.0610
0.7832	-0.0546
0.8188	-0.0481
0.8544	-0.0416
0.8900	-0.0351
0.9256	-0.0285
0.9612	-0.0219
0.9968	-0.0153
1.0324	-0.0086
1.0680	-0.0020
1.1036	0.0047
1.1392	0.0113
1.1748	0.0180
1.2104	0.0246
1.2460	0.0312
1.2816	0.0377
1.3172	0.0443
1.3528	0.0508
1.3884	0.0572
1.4240	0.0636
1.4596	0.0699
1.4952	0.0761
1.5308	0.0823
1.5664	0.0884
1.6020	0.0944
1.6376	0.1003
1.6732	0.1061
1.7088	0.1118
1.7444	0.1174
1.7800	0.1229
1.8156	0.1282
1.8512	0.1335
1.8868	0.1386
1.9224	0.1435
1.9580	0.1483
1.9936	0.1530
2.0292	0.1575
2.0648	0.1619
2.1004	0.1661
2.1360	0.1702
2.1716	0.1740
2.2072	0.1777
2.2428	0.1813
2.2784	0.1846
2.3140	0.1878
2.3496	0.1908
2.3852	0.1936
2.4208	0.1962
2.4564	0.1986
2.4920	0.2008
2.5276	0.2028
2.5632	0.2046
2.5988	0.2062
2.6344	0.2076
2.6700	0.2088
2.7056	0.2098
2.7412	0.2106
2.7768	0.2112
2.8124	0.2116
2.8480	0.2118
2.8836	0.2117
2.9192	0.2115
2.9548	0.2110
2.9904	0.2103
3.0260	0.2095
3.0616	0.2084
3.0972	0.2071
3.1328	0.2056
3.1684	0.2039
3.2040	0.2020
3.2396	0.1999
3.2752	0.1976
3.3108	0.1951
3.3464	0.1924
3.3820	0.1896
3.4176	0.1865
3.4532	0.1833
3.4888	0.1798
3.5244	0.1762
3.5600	0.1725
3.5956	0.1685
3.6312	0.1644
3.6668	0.1601
3.7024	0.1557
3.7380	0.1511
3.7736	0.1464
3.8092	0.1415
3.8448	0.1365
3.8804	0.1313
3.9160	0.1261
3.9516	0.1207
3.9872	0.1151
4.0228	0.1095
4.0584	0.1037
4.0940	0.0979
4.1296	0.0919
4.1652	0.0859
4.2008	0.0798
4.2364	0.0736
4.2720	0.0673
4.3076	0.0610
4.3432	0.0546
4.3788	0.0481
4.4144	0.0416
4.4500	0.0351
4.4856	0.0285
4.5212	0.0219
4.5568	0.0153
4.5924	0.0086
4.6280	0.0020
4.6636	-0.0047
4.6992	-0.0113
4.7348	-0.0180
4.7704	-0.0246
4.8060	-0.0312
4.8416	-0.0377
4.8772	-0.0443
4.9128	-0.0508
4.9484	-0.0572
4.9840	-0.0636
5.0196	-0.0699
5.0552	-0.0761
5.0908	-0.0823
5.1264	-0.0884
5.1620	-0.0944
5.1976	-0.1003
5.2332	-0.1061
5.2688	-0.1118
5.3044	-0.1174
5.3400	-0.1229
5.3756	-0.1282
5.4112	-0.1335
5.4468	-0.1386
5.4824	-0.1435
5.5180	-0.1483
5.5536	-0.1530
5.5892	-0.1575
5.6248	-0.1619
5.6604	-0.1661
5.6960	-0.1702
5.7316	-0.1740

2002 PY39 (cont'd)

Time(hr)	Relative Magnitude
5.7672	-0.1777
5.8028	-0.1813
5.8384	-0.1846
5.8740	-0.1878
5.9096	-0.1908
5.9452	-0.1936
5.9808	-0.1962
6.0164	-0.1986
6.0520	-0.2008
6.0876	-0.2028
6.1232	-0.2046
6.1588	-0.2062
6.1944	-0.2076
6.2300	-0.2088
6.2656	-0.2098
6.3012	-0.2106
6.3368	-0.2112
6.3724	-0.2116
6.4080	-0.2118
6.4436	-0.2117
6.4792	-0.2115
6.5148	-0.2110
6.5504	-0.2103
6.5860	-0.2095
6.6216	-0.2084
6.6572	-0.2071
6.6928	-0.2056
6.7284	-0.2039
6.7640	-0.2020
6.7996	-0.1999
6.8352	-0.1976
6.8708	-0.1951
6.9064	-0.1924
6.9420	-0.1896
6.9776	-0.1865
7.0132	-0.1833
7.0488	-0.1798
7.0844	-0.1762
7.1200	-0.1725
7.1556	-0.1685
7.1912	-0.1644
7.2268	-0.1601
7.2624	-0.1557
7.2980	-0.1511
7.3336	-0.1464
7.3692	-0.1415
7.4048	-0.1365
7.4404	-0.1313
7.4760	-0.1261
7.5116	-0.1207
7.5472	-0.1151
7.5828	-0.1095
7.6184	-0.1037
7.6540	-0.0979
7.6896	-0.0919
7.7252	-0.0859
7.7608	-0.0798
7.7964	-0.0736
7.8320	-0.0673